CHAPTER 4

DEOXYGENATION

4.1) INTRODUCTION

The presence of dissolved oxygen in samples often interferes in the application of electroanalytical methods. Oxygen from the atmosphere dissolves in water to produce concentrations of approximately 8.3 $mg.l^{-1}$ at 25°C (1 atm). This value was obtained by averaging a number of values given in the literature [1-3]. At this concentration a high background current is obtained on cathodic reduction of oxygen, which may obscure the analytical signal [4-7]. The dilemma would not be as dramatic if the presence of the oxygen waves were the only interference.

The reduction of oxygen proceeds via a hydrogen peroxide intermediate. In acidic solutions the mechanism is as follows [8]:

$O_2 + 2H^+ + 2e^- = H_2O_2$ $\quad E^0 = 0.69$ V

$H_2O_2 + 2H^+ + 2e^- = 2H_2O$ $\quad E^0 = 1.78$ V

and the overall reaction is:

$O_2 + 4H^+ + 4e^- = 2H_2O$ $\quad E^0 = 1.23$ V

In basic solutions the mechanism is:

$O_2 + 2H_2O + 2e^- = H_2O_2 + 2OH^-$ $\quad E^0 = -0.15$ V

$H_2O_2 + 2e^- = 2OH^-$ $\quad E^0 = 0.55$ V

and the overall reaction is:

$O_2 + 2H_2O + 4e^- = 4OH^-$ $\quad E^0 = 0.40$ V

The H_2O_2 intermediate can function as both an oxidising and reducing agent, and hence act on other electroactive species present. In unbuffered solutions, pH changes can occur in the vicinity of the electrode due to the electro-reduction of oxygen. A resultant increase in pH can lead to precipitation of heavy metal ions close to the electrode and therefore diminish their diffusion currents [4,5]. In stripping voltammetry, the oxygen present leads to the partial dissolution of the metal accumulated by preelectrolysis which lowers the results obtained [4,6].

Deoxygenation also prevents the following non-electrochemical process that can occur in a neutral, unbuffered metal salt solution containing metallic mercury and dissolved oxygen:

$$O_2 + 2Hg + 2Cl^- + 2H_2O = Hg_2Cl_2 + 4OH^- \qquad [4]$$

It is therefore the task of the electrochemist to remove the dissolved oxygen or to nullify the effects thereof, the former being the most widely used.

Sparging the solution with an inert gas is the most frequently used method of deoxygenation. This could, however, lead to sample evaporation and the loss of certain volatile components [6]. It also has limitations in flow analysis. This is mainly due to recontamination of the solution because oxygen can diffuse through the walls of the Teflon tubing generally used in flow analysis. Stainless steel tubing has been used as a substitution where possible, but this leads to metal contamination especially in harsh environments.

A chemical approach comprises of passing the solution through a reactor, in which a reagent that reacts with oxygen is immobilised. Pyrogallol (1,2,3-trihydroxybenzene) in alkaline solutions and ascorbic acid or columns packed with zinc particles in acidic solutions are examples of such reagents [4,6,9]. The drawback of this procedure is the introduction of impurities, particularly when doing trace analysis.

Photochemical methods have also been used. These are based on the reaction of oxygen with organic acids, such as formic, citric or oxalic acids, under UV irradiation. A high concentration of acid and a fairly long irradiation time is required to attain acceptable efficiency, hence this is not an elegant manner to deoxygenate a solution [4].

When determining elements with large negative standard potentials, such as zinc(II), oxygen can be reduced electrochemically prior to the analytical experiment [4,6]. This has a very limited use.

Changes in pressure or temperature can be employed to reduce the concentration of dissolved oxygen. The temperature of the solution can be increased, as the solubility of gases is inversely proportional to the temperature of the solution at a given pressure [4,6,7,9]. The solubility of sparingly soluble gases such as oxygen, nitrogen and carbon monoxide approaches zero at 100°C and ambient pressure [9]. Vacuum degassing and ultrasonication with an applied vacuum are also mechanisms used to reduce the amount of dissolved gases [4,7]. The applied vacuum decreases the pressure above the solution, thus allowing dissolved gases to expel from the solution and be removed by the vacuum [7]. This method could, however, also lead to sample evaporation and the loss of volatile components.

Gas permeable membranes through which the samples pass, with a reduced partial pressure of oxygen surrounding the membranes, have been used in a number of different ways [5-7]. The membrane can be surrounded by a strong reducing agent, such as chromium(II) in the presence of amalgamated zinc. As the oxygen diffuses through the membrane, it is scavenged by the reductant [6,7,10,11]. The mechanism is as follows [8]:

$$4Cr^{2+} + O_2 + 4H_3O^+ \rightarrow 4Cr^{3+} + 6H_2O$$

$$2Cr^{3+} + Zn(Hg) \rightarrow 2Cr^{2+} + Zn^{2+} + Hg$$

The membrane has also been surrounded by nitrogen or a vacuum, or both of these were applied together [4,5,6,11].

An inert gas, instead of air, could be used for segmenting flow streams to remove the dissolved oxygen from solution. The stream should first pass through a time delay coil to achieve more efficient deoxygenation [12]. Sample solutions were also mixed with large excesses of deaerated supporting electrolyte to minimise the effect of dissolved oxygen [4,12]. Neither of these procedures removed oxygen completely, although its concentration is markedly diminished as equilibrium is attained between the oxygen and nitrogen in the flow system [12].

The methods discussed thus far have all involved the removal of oxygen. Another approach is to discriminate against oxygen interference by choosing parameters such as the potential wave form, the chemical form of the analyte and the nature of the working electrode, such that it would alleviate the interference from dissolved oxygen [6].

4.2) SEMI-PERMEABLE MEMBRANES IN A NITROGEN ATMOSPHERE

The first experiments of gas diffusion through a membrane were employed for oxygenation of solutions. It was also a liquid-membrane-gas process. The driving force for the gas exchange was the difference in partial pressures. Eventually a steady state of the partial pressure of gases is reached [13]. This technology has now been employed in deoxygenators, particularly for flow systems.

There are two main properties to consider when choosing a membrane. Firstly, the membrane should be highly permeable to oxygen. The permeability coefficient for oxygen is equal to the product of the solubility coefficient of oxygen in the membrane and the diffusion rate of oxygen through the membrane. Secondly the membrane should be inert to the analyte solution [7,10,11]. In comparison to silicone, most other polymers are much less permeable to gases [4]. Silicone is also inert to a large variety of chemicals, thus making it a suitable membrane material. It is important to have a membrane with a small internal diameter and thin wall thickness to optimise the amount of deoxygenation.

There are numerous other factors affecting the extent of deoxygenation such as the temperature and the viscosity of the analyte solution, the volume ratio of gas to liquid, the pressure of the gas and the initial concentration of oxygen in the gas. The residence time, which is the quotient of the length of the membrane and the flow rate, also needs to be optimised [4,9,10].

Mass transfer by diffusion is the way of transporting a substance under the influence of a chemical potential gradient, generally being a concentration gradient, for stagnant fluids or fluids moving in laminar flow. This takes place at a much smaller rate than eddy or turbulent diffusion, which occurs when the fluid undergoes mechanical stirring or convective movement [12]. Fick's Law governs the rate of diffusion. It expresses the mass transfer rate per unit interfacial area (N_i) as a linear function of the molar concentration gradient.

$$N_i = -D \frac{dC_i}{dy}$$

where N_i is the molar flux of component i, dy is the distance over which the concentration gradient dC_i is present and D is the diffusion coefficient. The negative sign emphasises that diffusion occurs in the direction of the drop in concentration.

Thus Fick's Law can assist in predicting the time required to deoxygenate a solution to a degree suitable for the experiment [9,10,14].

The mass transfer in this membrane deoxygenation system is an important consideration. Firstly, consider a fluid flowing past a flat plate. The velocity at the solid surface is zero, so there must be a layer adjacent to the surface where the flow is predominantly laminar. Here the fluid can be thought of as being made up of thin layers sliding over each other at increasing velocities at increasing distances from the plate. The molecules in one layer, while travelling in their random directions, will move from a fast moving layer to an adjacent slower moving layer. Even when turbulent flow prevails, the layer adjacent to the surface in predominantly laminar. The character of the flow gradually changes as the distance from the surface increases [14]. Therefore Fick's Law should apply for diffusion across a membrane as the flow close to the surface of the membrane is laminar.

From Fick's Law, for diffusion through a flat slab of thickness z, the rate of diffusion per unit area (N) is given by:

$$N = \frac{D(C_1 - C_2)}{z}$$

where C_1 and C_2 are concentrations at opposite sides of the slab [14] and $C_2 > C_1$. The rate of diffusion for other shapes is given by [15]:

$$w = NS_{av} = \frac{DS_{av}(C_1 - C_2)}{z}$$

where S_{av} is the average cross section for diffusion. For radial diffusion through a solid cylinder of inner and outer radius r_i and r_o respectively, and of length ℓ: [14]:

$$S_{av} = \frac{2\pi\ell(r_o - r_i)}{\ln\left(\frac{r_o}{r_i}\right)}$$

and $z = r_o - r_i$

The diffusivity of oxygen in the liquid phase is much lower than that in the gas phase. This is due to resistance in the liquid phase [9,13]. Liquid resistance used to be considered the rate controlling resistance and the membrane resistance was ignored. Tang *et al.* showed the significance of membrane resistance to gas transfer under various operating conditions [13]. Thus, when diffusion through a solid occurs, the structure of the solid and its interaction with the diffusing substance have a profound influence on how diffusion takes place and on the rate of transport [14]. Solid materials through which diffusion can occur are polymers, crystalline solids and porous solids. Since a silicone membrane is a polymer, the mechanism by which diffusion occurs through a polymer will be looked at more closely. Diffusion of solutes through polymeric substances is generally similar to diffusion through liquid solutions, especially for gas solutes. The gas dissolves in the solid at the faces exposed to the fluids and then diffuses from the high to low concentration side of the polymer. The polymeric chains are in a state of constant thermal motion and the diffusing molecules move from one position to another over the potential barrier. A successful move requires that there is an available hole or passage of sufficient size, which in turn depends on the thermal motion of the polymer chains. Therefore diffusion depends on the temperature. In the case of oxygen and nitrogen, the molecules are relatively small, so diffusion is relatively easy [14].

4.3) EXPERIMENTAL

A semi-permeable membrane deoxygenation system was used in this study because it was an efficient way to remove oxygen, particularly for a flow system, and it was also inexpensive and fairly easy to implement. The deoxygenation system consisted of a 3 m length of gas permeable silicone tubing placed inside the same length of impermeable polyethylene tubing. The silicone tubing had an internal diameter of

0.75 mm and a wall thickness of 0.25 mm (Carlin Medical Extrusions, Eden Glen, Johannesburg) and the polyethylene tubing had an internal diameter of 3.8 mm and a wall thickness of 1.2 mm (Controlled Irrigation, Bramley, Johannesburg). A counter flow system, as illustrated in figure 4.1, where the solution flowing through the silicone tubing flows in the opposite direction to the nitrogen flowing in the polyethylene tubing, was used. In this way a concentration gradient for oxygen is maintained throughout the entire length of the tubing, improving the deoxygenation efficiency.

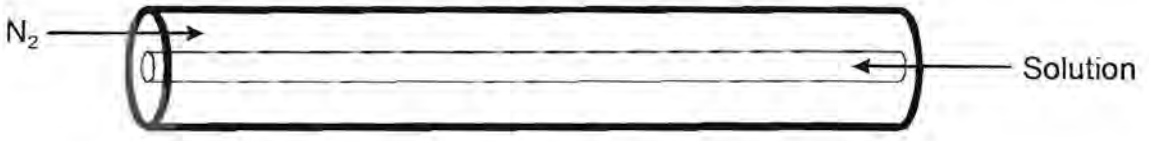

Figure 4.1: Schematic diagram of a counter flow deoxygenation system

Since the nitrogen in the gas cylinder may have contained small quantities of oxygen, the gas was scrubbed. Two scrubbers were employed. The first scrubber contained a vanadous chloride solution with some amalgamated zinc. The vanadous chloride was prepared by boiling 2 g of ammonium metavanadate with 25 ml hydrochloric acid and then diluted to 250 ml. The amalgamated zinc was prepared by covering zinc filings with deionised water, adding 2 drops of hydrochloric acid and then adding mercury. A blue-green solution was produced which turned purple when nitrogen was bubbled through it. When it was exhausted it turned a blue green colour once again. The solution could be rejuvenated by the addition of more amalgamated zinc or a few drops of hydrochloric acid [15]. The mechanism by which the scrubber removed oxygen is:

$$4V^{3+} + O_2 + 4H_3O^+ \rightarrow 4V^{4+} + 6H_2O$$

$$4V^{4+} + 2Zn(Hg) \rightarrow 4V^{3+} + 2Zn^{2+} + 2Hg$$

The second scrubber contained deionised water to trap any vanadous chloride. It was found that gas scrubbing played an important role when the difference in currents were

observed for a new scrubber versus an exhausted one. The flow rate of nitrogen was also estimated by observing the amount of bubbling occurring in the scrubbers.

This membrane deoxygenation system was part of the flow system as shown in chapter 5. It was used with both the flow cell for the SMDE and the WJC. It was tested in both cases due to the different demands of the set-ups.

4.3.1) Testing Deoxygenation using the Flow Cell for the SMDE

In order to investigate the extent of deoxygenation, a solution was tested before and after deoxygenation and the difference in the voltammograms noted. A 0.5 $mol.l^{-1}$ sulphuric acid solution was considered first. Although the effect of deoxygenation was evident, it was difficult to quantify the amount of deoxygenation that had taken place. A copper solution in 1 $mol.l^{-1}$ nitric acid was then tested. The copper reduction peak is close to the first reduction peak of oxygen, thus in a solution exposed to the atmosphere the oxygen peak predominates resulting in the inability to detect the copper [16]. A concentration of 1 $mg.l^{-1}$ copper was first used, but proved to be too high as it diminished the effect of dissolved oxygen in the solution, so a 20 $\mu g.l^{-1}$ copper concentration was used. The differential pulse stripping voltammetry (DPSV) mode was used with the parameters as follows:

initial potential = –300 mV
final potential = 120 mV
deposition time = 180 s
quiet time = 10 s
scan rate = 20 $mV.s^{-1}$
pulse amplitude = 50 mV
sample width = 20 ms
pulse width = 50 ms
pulse period = 200 ms

The effects of the presence of dissolved oxygen, particularly for trace concentration determination, can readily be seen in figure 4.2.

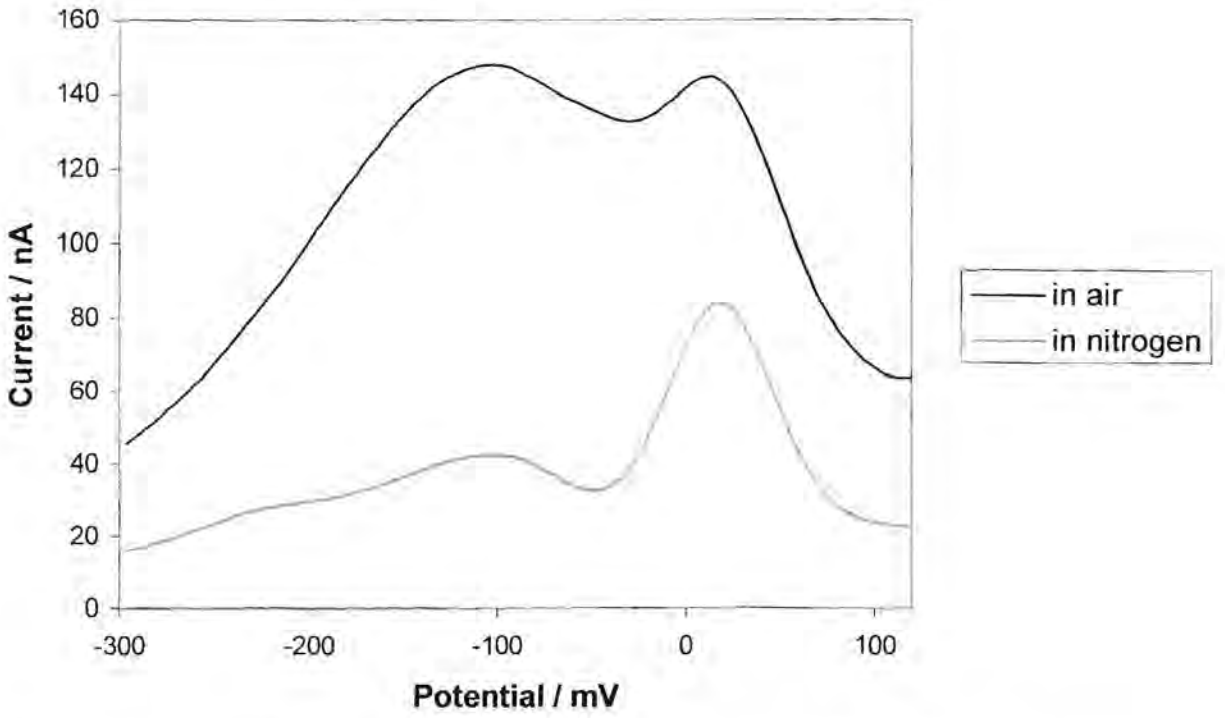

Figure 4.2: 20 $\mu g.l^{-1}$ Cu in 1 $mol.l^{-1}$ HNO_3 measured in an air atmosphere and then in a nitrogen atmosphere

Finally the method used by Pedrotti *et al.* [4], who employed a sodium perchlorate solution under hydrodynamic conditions, was used. A 10 $mmol.l^{-1}$ $NaClO_4$ (that had been recrystallised) solution was made. Linear sweep voltammetry (LSV) was used to collect the data from 200 mV to –1400 mV. A scan rate of 10 $mV.s^{-1}$ and sensitivity of 1 $\mu A.V^{-1}$ was used. Data were collected while the pump was running at a speed setting of 10 which corresponded to 1.5 $ml.min^{-1}$ (see chapter 5). Figure 4.3 shows the difference in currents for an oxygenated versus a deoxygenated solution. The efficiency of oxygen removal was evaluated from the ratio of the initial current before deoxygenating and the steady state current afterwards. Since the deoxygenation system consisted of a long tube, it was necessary to first flush the polyethylene tubing with nitrogen for some time to purge all the oxygen out. It was found that a 30 minute flush was sufficient as longer periods had no further significant effect.

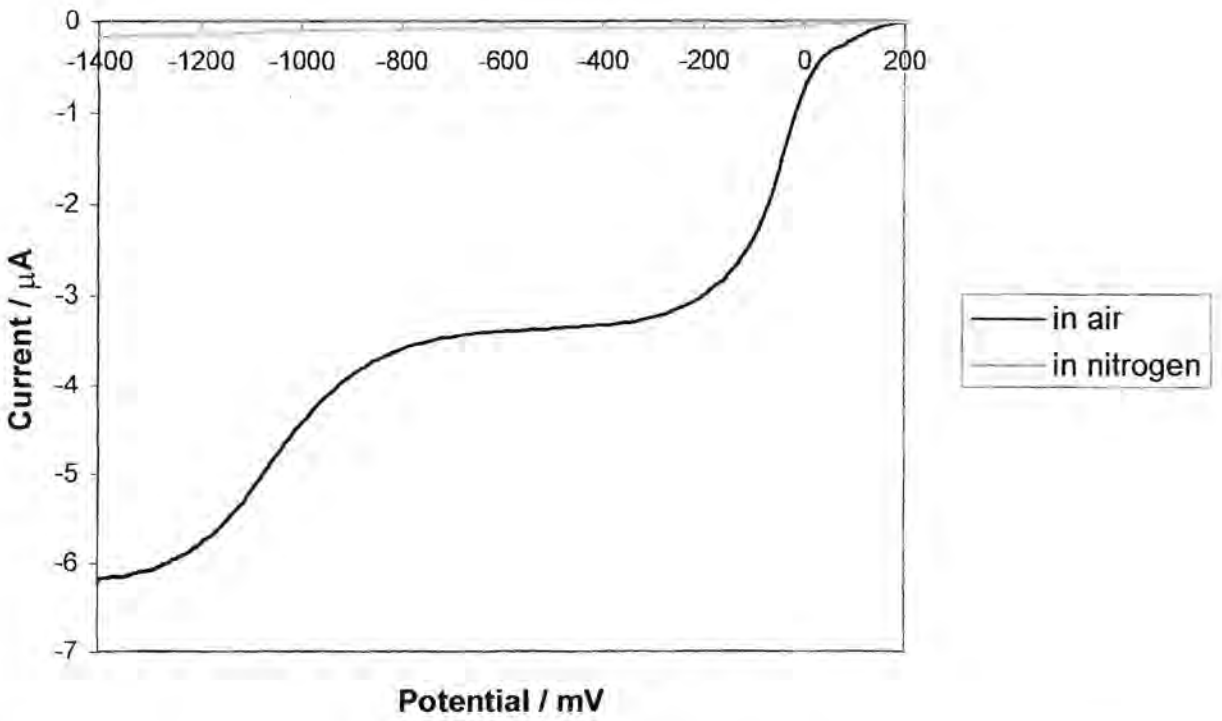

Figure 4.3: The oxygen reduction current in 1 mmol.l^{-1} $NaClO_4$ measured in an air atmosphere and then in a nitrogen atmosphere

Three different deoxygenation set-ups were tested, namely:

1) the deoxygenation tubing alone,
2) the deoxygenation tubing together with sparging the solution in a flask before entering the tubing, and
3) sparging the solution in the flask alone before passing directly into the flow cell.

The steady state currents were measured at -550 mV and the results are presented in table 4.1.

Table 4.1: Deoxygenation efficiencies

Atmosphere	Air	Nitrogen		Air	Nitrogen
Set-up	Tubing	Tubing	Tubing + Flask	Flask	Flask
Steady state current (nA) at -550 mV	3.37×10^3	72.0	39.1	4.27×10^3	372
Current decrease factor	1	47	86	1	11
Residual dissolved O_2 ($\mu g.l^{-1}$)	8.3×10^3	177	96.5	8.3×10^3	755
O_2 removal efficiency (%)		97.9	98.8		90.9

Where:

$$\text{current decrease factor} = \frac{\text{steady state current in air}}{\text{steady state current in nitrogen}}$$

$$\text{residual dissolved } O_2 = \frac{8.3 \times 10^3 \ \mu g.l^{-1}}{\text{current decrease factor}}$$

$$O_2 \text{ removal efficiency} = \frac{8.3 \times 10^3 - \text{residual dissolved } O_2}{8.3 \times 10^3} \times 100\,\%$$

The concentration of dissolved oxygen given as 8.3 $mg.l^{-1}$ is the value for distilled water. This concentration decreases as the concentration of the electrolyte increases [17]. In addition, oxygen is non-polar and hence becomes less soluble as the solvent polarity increases [7]. The dissolved oxygen concentration should thus be significantly lower for the concentrated electrolytes used in this study.

In the case of the flask set-up, a pulse damper, as described in chapter 5, was placed between the pump and the flow cell when the deoxygenation tubing was removed. Data in air was also collected for this set-up as the hydrodynamics may have varied slightly

in the absence of the tubing. A point was reached where increasing the sparging time did not affect the current measured. This proved to be the least efficient method for oxygen removal which was probably due to contamination while passing through the Teflon tubing of the pump which is susceptible to gas diffusion. The pulse damper could also have been a source of contamination as the sealed tube that was perpendicular to the solution flow contained air.

The most efficient method of oxygen removal was using the combination of sparging the solution in the flask before passing into the tubing. The bulk of the oxygen was removed during the sparging and the tubing set-up could remove further traces. Any contamination from passing through the Teflon pump tubing was also removed in the deoxygenation tubing. It was decided, however, that this method would be impractical and time consuming. An alternative would have been to only sparge the stripping electrolyte which would reduce the oxygen signal. However, the oxygen removal efficiency was only one percent lower if sparging was not done first, so the tubing set-up alone was used.

4.3.2) Testing Deoxygenation using the Wall-Jet Cell

The method that was used by Pedrotti *et al.* [4] and in the previous section was tested at the gold film electrode in the wall-jet cell (WJC). Measurements were made firstly in an air atmosphere and then, after flushing the tubing for 30 minutes, measurements of the deoxygenated solutions were made at various flow rates. 10 $mmol.l^{-1}$ sodium perchlorate was pumped through the system and LSV was done between 400 mV and –500 mV at a scan rate of 10 $mV.s^{-1}$. The results are presented in figure 4.4. There was a definite decrease in current at the lower potentials after deoxygenation. Varying the flow rate while deoxygenating yielded at least two variables, namely, as the flow rate increased, the rate at which the analyte was transferred to the electrode increased and the rate of deoxygenation decreased due to a reduced time spent in the deoxygenation system. A third possible variable would be the performance of the wall jet, in other words, was the flow rate fast enough to produce a stable jet and so on. It

was difficult to quantify the extent of deoxygenation in this case, so other options were considered.

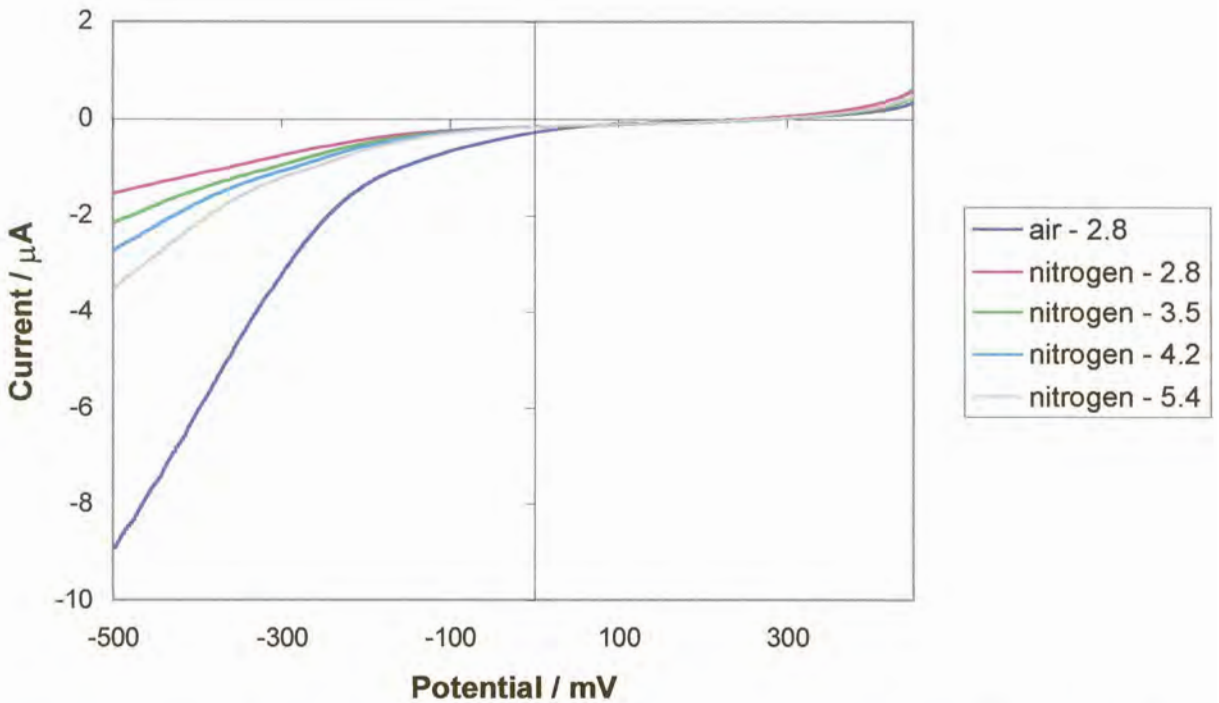

Figure 4.4: The oxygen reduction current in 1 mmol.l^{-1} $NaClO_4$ measured in an air atmosphere and then in a nitrogen atmosphere at varying flow rates (in ml.min^{-1}) at a gold film electrode

A 1 mg.l^{-1} copper solution containing 0.1 mol.l^{-1} potassium nitrate was then studied and the peak currents were measured. DPSV was applied between -300 mV and 200 mV at a scan rate of 20 mV.s^{-1} after a deposition time of 5 s at -300 mV. The other parameters were the default values as used in the previous section. The presence of oxygen would result in a higher background current and hence a smaller copper peak. Deoxygenation took place firstly in the tubing only and then in the tubing after sparging the solution in a flask. In the latter case, sparging with nitrogen first took place for 30 minutes before the analyses began. The results depicted in figure 4.5 clearly show the effect of deoxygenation. Deoxygenation merely through the tubing was not sufficient as the responses increased with additional deoxygenation in the flask. When the solution was

deoxygenated in the tubing only, the slope of the line was slightly greater than that in air. This indicates that the faster copper mass transport, which would increase the peak current, balanced with the reduced deoxygenation at higher flow rates, which would decrease the peak current. However, when deoxygenation took place in both the flask and the tubing, the slope increased to a greater extent. In this case smaller amounts of oxygen needed to be removed, so at the greater flow rates, the extent of mass transport predominated. It was thus evident that at higher flow rates, the tubing system was not sufficient on its own.

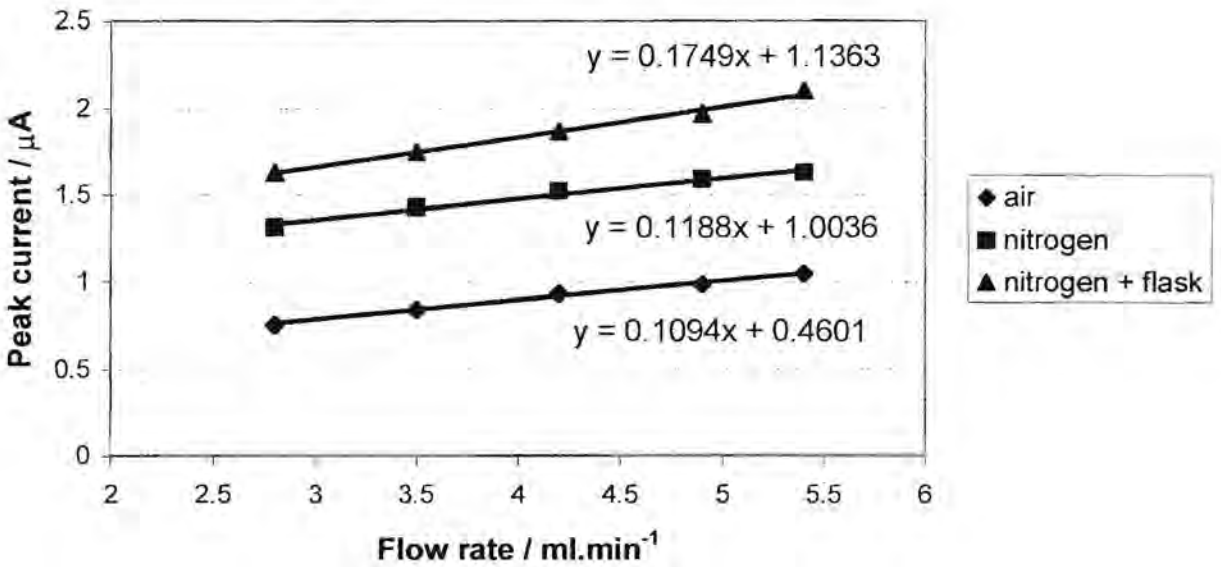

Figure 4.5: Graph of peak current versus flow rate for a 1 $mg.l^{-1}$ copper solution in an air atmosphere and then after deoxygenation in both the tubing system and a flask + the tubing system

Lastly, the GCE was plated with a mercury film and the method by Pedrotti *et al.* [4] was attempted again. The mercury film was plated from a 1.4 $mmol.l^{-1}$ Hg^{2+} (added as $HgCl_2$) solution containing 8 $mmol.l^{-1}$ hydrochloric acid. This was done in a cup cell while stirring the solution. The film was deposited at –1200 mV for 60 s. Data were collected using LSV between 100 mV and –1400 mV at 10 $mV.s^{-1}$. The voltammograms in figure 4.6 clearly show the reduced background current due to deoxygenation, which only took place in the tubing, and the results are presented in table 4.2. These showed

that at lower flow rates, the extent of deoxygenation was greater. A flow rate of 4.2 $ml.min^{-1}$ was used in the WJC (see chapter 5) which led to a deoxygenation efficiency of 94.7%.

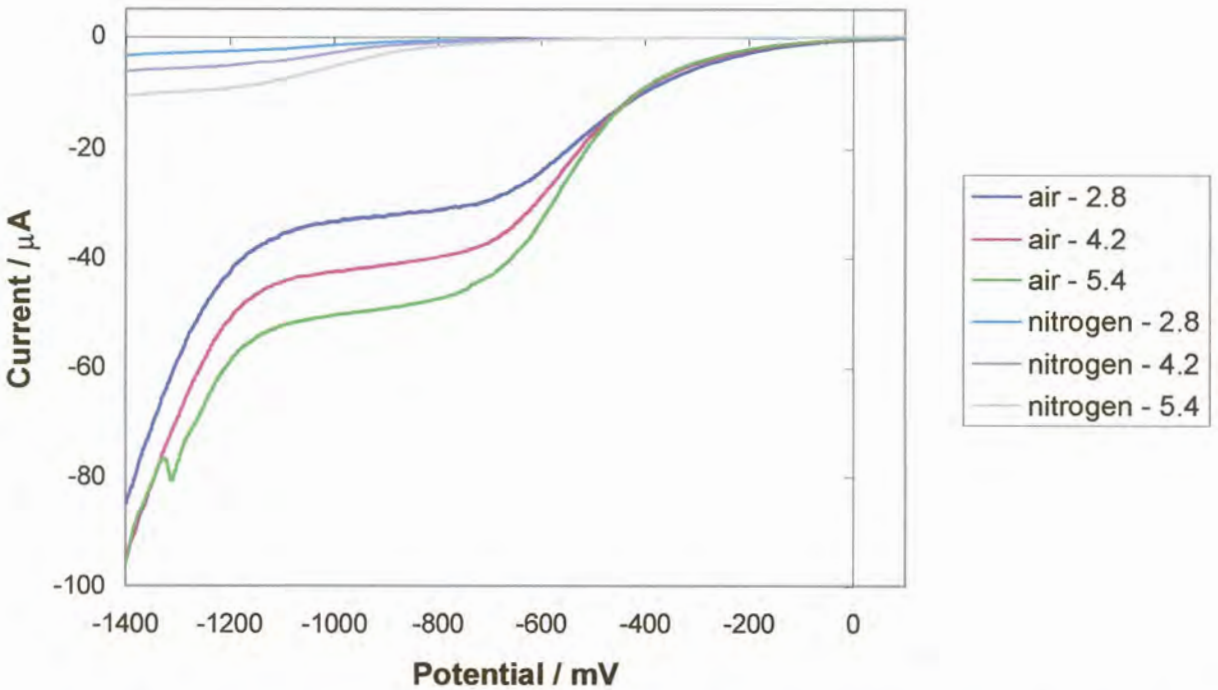

Figure 4.6: The reduction of oxygen in 1 $mmol.l^{-1}$ $NaClO_4$ measured in an air atmosphere and then in a nitrogen atmosphere at varying flow rates (in $ml.min^{-1}$) at a mercury film electrode

Table 4.2: Deoxygenation efficiencies

Atmosphere	Air			Nitrogen		
Flow rate ($ml.min^{-1}$)	2.8	4.2	5.4	2.8	4.2	5.4
Steady state current (μA) at –950 mV	32.8	42	50.1	1.28	2.21	4.24
Current decrease factor	1	1	1	25.6	19.0	11.8
Residual dissolved O_2 ($\mu g.l^{-1}$)	$8.3x10^3$	$8.3x10^3$	$8.3x10^3$	324	437	702
O_2 removal efficiency (%)				96.1	94.7	91.5

The gold samples that were to be analysed for arsenic were dissolved in alkaline cyanide solutions in the presence of oxygen. It was feared that the excess cyanide in the alkaline sample solution would attack the gold film electrode if there was still oxygen (be it only about 440 $\mu g.l^{-1}$ oxygen) present. This would lead to rapid electrode degradation and irreproducible results. In order to improve deoxygenation, the tubing could be lengthened to increase the residence time of the solution in the deoxygenation system, however, this could lead to severe dispersion problems. Purging the solutions in a flask beforehand seemed to be the best option. This was done using a separate nitrogen cylinder and inserting a number of T-pieces between the tubing so that several samples could be purged simultaneously. This ensured that the analysis time was not extended unnecessarily which could also lead to the electrode degrading on standing for prolonged periods in the sample solutions.

4.4) DISCUSSION

The semi-permeable membrane deoxygenation system was a convenient way to deoxygenate samples in a flow system. It was very efficient in oxygen removal and not

at all time consuming. The degree of deoxygenation efficiency depended on the flow rate on the solution, and at higher flow rates this method was supplemented by purging the samples beforehand. This, however, would not always be necessary and would depend on the experimental requirements. It also functioned as a pulse damper. The drawbacks of using this system were that work had to be done within the constraints of the tubing length and the extent of dispersion also increased.

4.5) REFERENCES

1) G.W. Kaye and T.H. Laby, Tables of Physical and Chemical Constants (15th ed.), Longman Group Ltd, 1986

2) W.F. Linke, Solubilities – Inorganic and Metal-Organic Compounds (4th ed.), Vol. 1, American Chemical Society, 1958

3) W.F. Linke, Solubilities – Inorganic and Metal-Organic Compounds (4th ed.), Vol. 2, American Chemical Society, 1958

4) J.J. Pedrotti, L. Angnes and I.G.R. Gutz, Anal. Chim. Acta, 298 (1994) 393

5) Trojanek and K. Holub, Anal. Chim. Acta, 121 (1980) 23

6) G.G. Wallace, Trends in Anal. Chem., 4 (1985) 145

7) M.E. Rollie, G. Patonay and I.M. Warner, Ind. Eng. Chem. Res.,26 (1987) 1

8) Colombo and C.M.G. van den Berg, Anal. Chim. Acta, 377 (1998) 229

9) X.-S. Chai and L.-G. Danielsson, Anal. Chim. Acta, 332 (1996) 31

10) M.E. Rollie, G. Patonay and I.M. Warner, Anal. Chem., 59 (1987) 180

11) R.E. Relm, Anal. Chem., 55 (1983) 1188

12) W. Lund and L.-N. Opheim, Anal. Chim. Acta, 79 (1975) 35

13) T.E. Tang and S.-T. Hwang, AIChE Journal, 22 (1976) 1000

14) R.E. Treybal, Mass-Transfer Operations (3rd ed.), McGraw-Hill Inc., Singapore, 1980

15) Model 303 static mercury drop electrode operating and service manual, EG&G Princeton Applied Research, Princeton, 1978

16) J.F. van Staden and M. Matoetoe, Fresenius J. Anal. Chem., 357 (1997) 624

17) H. Eskilsson, C. Haraldsson and D. Jagner, Anal. Chim. Acta, 175 (1985) 79

CHAPTER 5

FLOW SYSTEMS

The flow system incorporates both the flow cell and the deoxygenation system and how they operate together. It also includes the control of the pump and valve, as well as data collection.

5.1) THEORY

A large number of cell geometries with forced convection have been designed. The general equation, in Cartesian coordinates, to describe the mass transfer of an electroactive species by convective diffusion is [1]:

$$\frac{\partial c}{\partial t} = D\left(\frac{\partial c}{\partial x} + \frac{\partial c}{\partial y} + \frac{\partial c}{\partial z}\right) - \left(V_x\frac{\partial c}{\partial x} + V_y\frac{\partial c}{\partial y} + V_z\frac{\partial c}{\partial z}\right)$$

where D is the diffusion coefficient and V_x, V_y, and V_z are the velocity distribution functions. The first group of terms refers to the diffusive mass transfer and the second group to the convective mass transfer processes. The influence of migration is ignored as it is negligible when the electroactive species contributes negligibly to the ionic strength.

The limiting current can be written as [2]:

$$i_\ell = nFI_{max}$$

where I_{max} is the maximum diffusion mass flow towards the electrode surface, n is the number of electrons involved and F is Faraday's constant. It is therefore necessary to describe the diffusion towards the electrode in order to find the limiting current. Equations for the limiting currents under steady-state conditions have been derived for various cell geometries as shown in figure 5.1 [1]. These are displayed in table 5.1 [1].

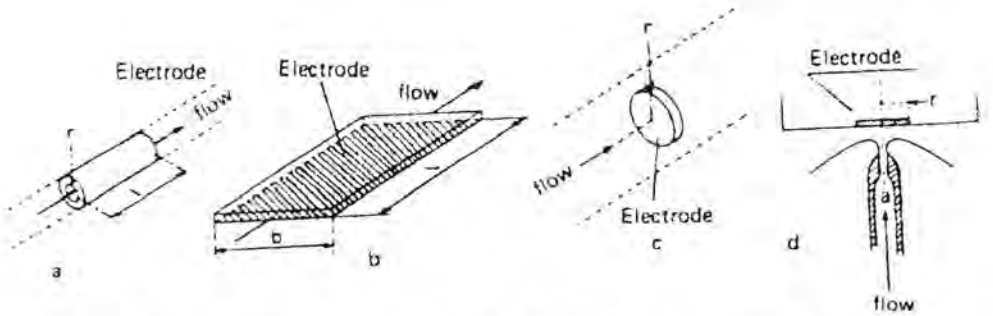

Figure 5.1: Electrode geometries for flow systems with electrochemical detection: a) tubular, b) planar with parallel flow, c) planar with perpendicular flow and d) wall-jet

Table 5.1: Limiting current equations for various cell geometries

Electrode geometry	**Limiting current equation**
Planar (parallel flow)	$i = 0.68\, nFCD^{\frac{2}{3}}\nu^{-\frac{1}{6}}\left(\frac{A}{b}\right)^{\frac{1}{2}}V^{\frac{1}{2}}$
Thin layer	$i = 1.47\, nFC\left(\frac{DA}{b}\right)^{\frac{2}{3}}V^{\frac{1}{3}}$
Planar (perpendicular flow)	$i = 0.903\, nFCD^{\frac{2}{3}}\nu^{-\frac{1}{6}}A^{\frac{3}{4}}u^{\frac{1}{2}}$
Wall-jet	$i = 1.38\, nFCD^{\frac{2}{3}}\nu^{-\frac{5}{12}}a^{-\frac{1}{2}}R^{\frac{3}{4}}V^{\frac{3}{4}}$
Tubular	$i = 1.61\, nFC\left(\frac{DA}{r}\right)^{\frac{2}{3}}V^{\frac{1}{3}}$

where i = limiting current (A)

n = number of electrons

F = Faraday constant ($C.mol^{-1}$)

C = concentration ($mol.l^{-1}$)

D = diffusion coefficient ($m^2.s^{-1}$)

A = electrode area (m^2)

r = radius of tubular electrode (m)

V = average volume flow rate ($m^{-3}.s^{-3}$)

ν = kinematic viscosity ($m^2.s^{-1}$)

b = channel height (m)

R = electrode radius (m)

a = diameter of inlet (m)

u = velocity ($m.s^{-1}$)

The relationships in these hydrodynamic situations apply only to laminar flow, not turbulent flow. The dimensionless Reynolds number, Re, characterises the transition from laminar to turbulent flow. It is the ratio of inertial and viscous forces for a particular electrode geometry and is given by [2]:

$$Re = \frac{Ul}{\nu}$$

where U is the velocity, l is the length and ν is the kinematic viscosity. A critical Reynolds number, Re_{Cr}, indicates the onset of turbulent flow. Thus for laminar flow $Re < Re_{Cr}$ [1]. For example, $Re_{Cr} = 1000$ for a WJC. Laminar flow is also necessary for a low amount of noise [1].

When a fluid flows over the electrode surface, a very thin layer is formed at the surface where the velocity gradient normal to the surface is very large. This layer is called the boundary layer [1,3]. The boundary layer thickness is dependant on the design of the flow cell and is important to optimise the detector's performance. The thickness of the diffusion layer, which defines the concentration gradient at the electrode surface, is a few percent of the boundary layer. Levich approximated the relationship as [1]:

$$\delta_{dl} = \left(\frac{D}{\nu}\right)^{\frac{1}{3}} \delta_{bl}$$

where δ_{dl} is the thickness of diffusion layer, δ_{bl} is the thickness of boundary layer, D is the diffusion coefficient and ν is the kinematic viscosity.

When pumping solutions through the tubing in a flow system, dispersion of the solutions occur. This dispersion depends both on convection and diffusion. It is agreed that convection plays a greater role straight after injection and that diffusion is dominant after a certain time period [4]. A solution moving under laminar flow may be thought of as having a classical parabolic velocity profile which adopts a bullet shape with a hollow tail, as illustrated in figure 5.2(a) and 5.2(b) [5]. This would lead

to rapid dispersion, but radial diffusion reduces this effect. The tip of the slug diffuses outwards to the slower moving solution and is thus retarded. Also, the tail of the slug diffuses inwards into faster moving streams and is accelerated to produce a slug as shown in figure 5.2(c) [5]. There seems to be some conflicting ideas whether the dispersion of a sample zone increases or decreases with decreasing flow rate, but the dominant thought is that dispersion would decrease. For stopped flow systems, the dispersion is practically independent of the time that the flow is ceased [4].

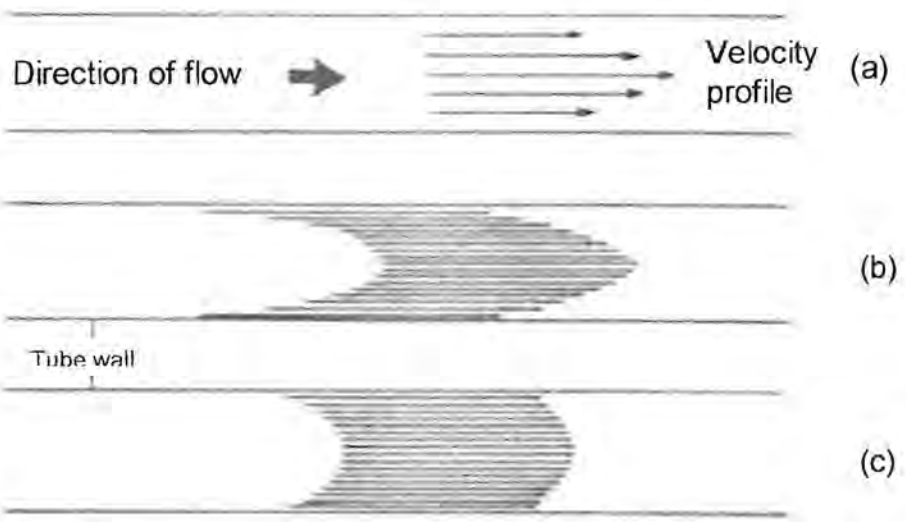

Figure 5.2: Dispersion of a sample slug in a flowing stream: (a) laminar flow velocity profile, (b) dispersion of sample slug caused by convection and (c) sample zone modified by diffusion.

In segmented flow systems, gas bubbles are introduced between slugs to avoid excessive dispersion. The only mixing that occurs is due to the adherent thin film left behind by the solution on the inner tube wall, but this is generally insignificant [6]. The problem with segmented flow is that the bubbles may need to be removed depending on the detector used and their compressibility also creates difficulties.

5.2) DATA COLLECTION

5.2.1) Potential Waveforms

Voltammetry was the electroanalytical technique used in this project. There are a number of variants of the waveforms in this technique, such as linear sweep

voltammetry (LSV), cyclic voltammetry (CV), pulse voltammetry, square wave voltammetry (SWV) and so on. In voltammetry the potential is varied in a defined manner and the current response is monitored [7].

LSV involves varying the potential linearly from an initial to a final value at a constant scan rate, as illustrated in figure 5.3 [7]. However, in practice, this potential waveform is a staircase as a true linear waveform is impossible to generate digitally. The drawbacks of using LSV are the relatively low resolution and the unfavourable effect of the charging current, which interferes especially in the determination of very low concentrations of substances by distorting the stripping curves [8]. CV is a variation of LSV where the scan direction is reversed when the final potential is reached and the scan occurs in the opposite direction. It is frequently used to characterise a redox system and is used to study the kinetics and the mechanism of a system [7].

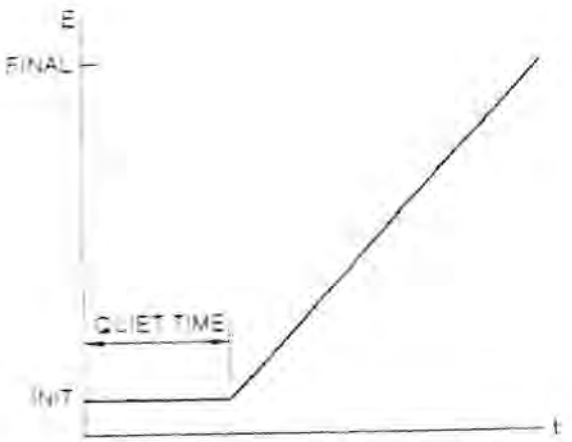

Figure 5.3: Potential waveform for LSV

The BAS workstation offers both normal pulse voltammetry (NPV) and differential pulse voltammetry (DPV). NPV has a waveform that consists of a series of pulses of increasing amplitude, with the potential returning to the initial value between pulses, as demonstrated on figure 5.4 [7]. When the initial potential is significantly positive of the reduction potential, the application of a small pulse does not cause a faradaic reaction, in other words a reaction which involves charge transfer across the electrode-solution interface. When the pulse potential is sufficiently large to cause a faradaic reaction, the magnitude of the current increases. This may be dependent on

both diffusion and the rate of electron transfer. A limiting current is reached when the electron transfer occurs rapidly at sufficiently negative potentials. The current-potential curve produced is thus sigmoidal in shape. In DPV the base potential increases in small steps and the pulse amplitude is constant with respect to the base potential, as shown in figure 5.5 [7]. The current is sampled twice in this technique, just before the pulse and at the end of the pulse. The difference of these currents is then recorded as a function of the base potential. Once again, at potentials significantly positive of the redox potential, there is no faradaic reaction when the pulse is applied. This results in a zero differential current. At potentials around the redox potential, the differential current reaches a maximum and then decreases to zero as the current becomes diffusion controlled. This results in a symmetric peak-shaped curve for the current-potential plot. In this manner DPV is able to discriminate against the charging current [7].

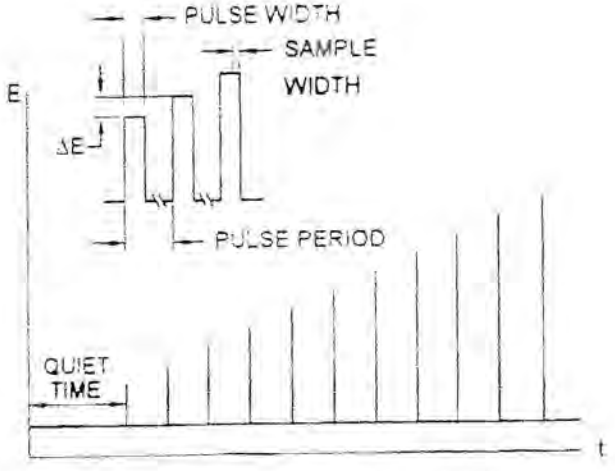

Figure 5.4: Potential waveform for NPV

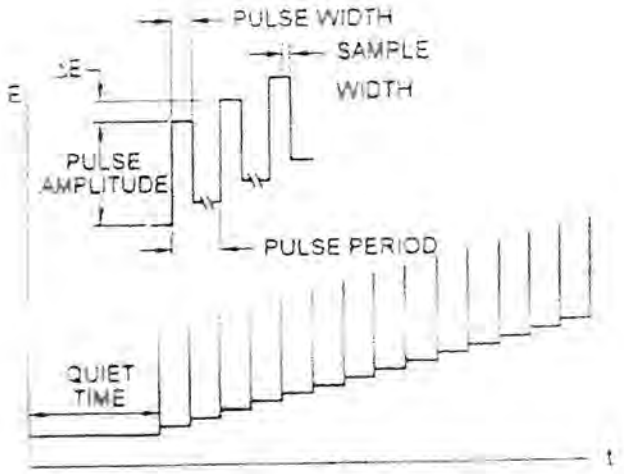

Figure 5.5: Potential waveform for DPV

There are two square waveforms available on the BAS workstation, namely the Osteryoung SWV (OSWV) and the Barker SWV (BSWV). The potential waveform for OSWV is a series of pulses alternating in direction as shown in figure 5.6 [7]. The current is sampled at the end of each pulse or half-cycle. The forward current, reverse current and the difference between these can be viewed. The differential current response is also a symmetric peak with discrimination against background charging currents. The technique has a greater sensitivity and faster speed than DPV [7]. BSWV is similar to OSWV, except the samples are collected and averaged over a number of cycles (as illustrated in figure 5.7), thus making it slower than OSWV [11].

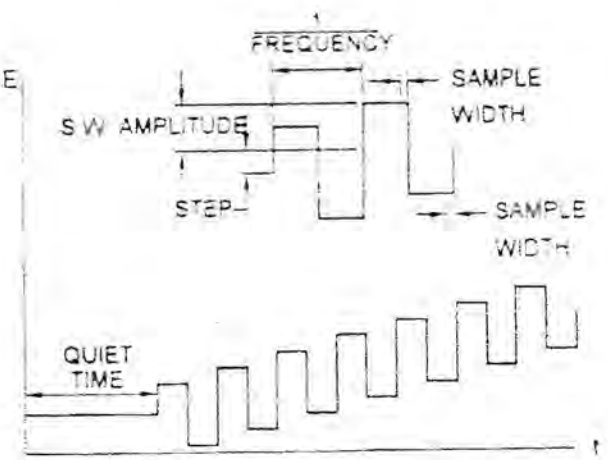

Figure 5.6: Potential waveform for OSWV

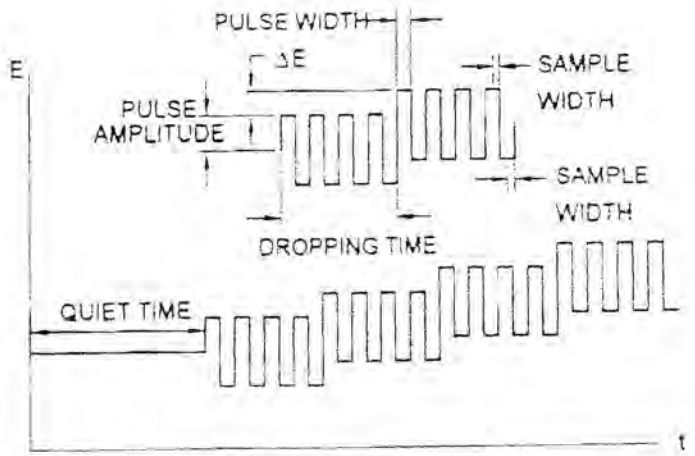

Figure 5.7: Potential waveform for BSWV

The waveforms discussed above (except for CV) can all be applied to stripping voltammetry. This is when the analyte is first accumulated onto or into the electrode as discussed in chapter 1. The analyte is accumulated at a given potential and then the waveform is applied during the stripping step. This enhances sensitivity and hence allows for very low detection limits [7].

In this work, DPV was mainly used due to its sensitivity and ease of use. OSWV was also briefly looked at. It proved to be more sensitive, but more complex to produce a well-defined peak.

5.2.2) iR Compensation

iR compensation was used in all experiments. This was necessary as it could have affected the true value of the operating potential of the cell. This is demonstrated by considering an electrochemical cell as represented in figure 5.8.

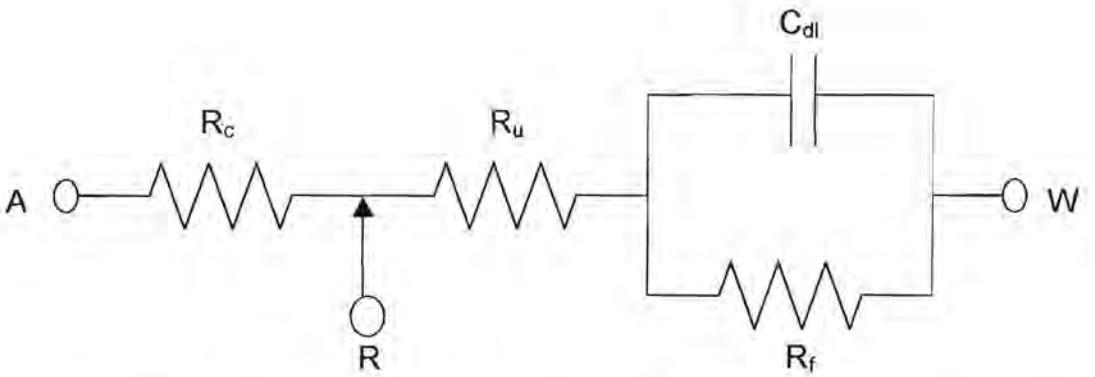

Figure 5.8: Equivalent circuit of an electrochemical cell. A = auxillary electrode, R = reference electrode, W = working electrode, R_c = compensated resistance, R_u = uncompensated resistance, R_f = faradaic impedance and C_{dl} = double layer capacitance [9].

The potential applied (E_{app}) across the reference and working electrodes is related to the true operating potential (E_w) across the working electrode and the solution interface by:

$$E_w = E_{app} - iR_u - \varphi_{ref}$$

where ϕ_{ref} is the reference electrode interfacial potential

or E_w (vs ref) = $E_{app} - iR_u$

If iR_u is large, it would substantially lower E_w from E_{app}, thus making the data obtained meaningless. There are generally three ways to minimise iR drop, namely: using a highly concentrated electrolyte, placing the reference electrode as close to the working electrode as possible and having an adjustable positive feedback (f) in the potential control loop such that E_w is related to the other circuit components as follows:

$$E_w \text{ (vs ref)} = E_{app} - iR_u + ifR_u$$

The positive feedback is gradually increased until the current response starts to oscillate. At this point $iR_u = ifR_u$ and the solution resistance is assumed as totally compensated for. However, this does not necessarily lead to 100% compensation as the circuit may become unstable before this is achieved. Another drawback of using this method is that the electrode surface structure may be destroyed or altered when the system starts to oscillate [9].

The BAS potentiostat uses a different approach to solve this problem [9]. Firstly a test potential is required where only capacitive response would occur at the working electrode and solution interface, i.e. no faradaic processes should occur. The instrument applies a potential step of 50 mV to the working electrode at this potential and then monitors the current response as follows:

$$i = i_o \exp\left(-\frac{t}{R_u C_{dl}}\right)$$

Two data points are sampled at 54 and 72 μs respectively and are assumed to be shorter than the R_uC_{dl} time constant. The exponential current decay can be approximated with a linear plot under this circumstance. It is extrapolated to t_o and the uncompensated resistance can hence be calculated using:

$$R_u = \frac{\Delta E}{i_o}$$

where ΔE is the potential step applied. The instrument then stepwise inserts a fraction of R_u in the positive feedback loop and tests the circuits stability. The stability test is performed by once more applying a potential step of 50 mV to the working electrode at the given test potential. The current response is then sampled at a frequency of 20 kHz for 50 ms. The maximum and minimum current is found and used to calculate the % overshoot as follows:

$$\%\,\text{overshoot} = \frac{i_{min}}{i_{max}} \times 100$$

This procedure is repeated until iR compensation is achieved in accordance with preset levels of both overshoot and compensation extent [9]. (The default values of 10% and 100% respectively, were used in this work.) The instrument now slightly decreases the iR compensation and inserts a capacitor between the auxilliary and reference leads to stabilise the cell system.

5.3) FLOW SYSTEM FOR THE SMDE

5.3.1) Set-up

The set-up for the experimental work in this study is depicted in figure 5.9.

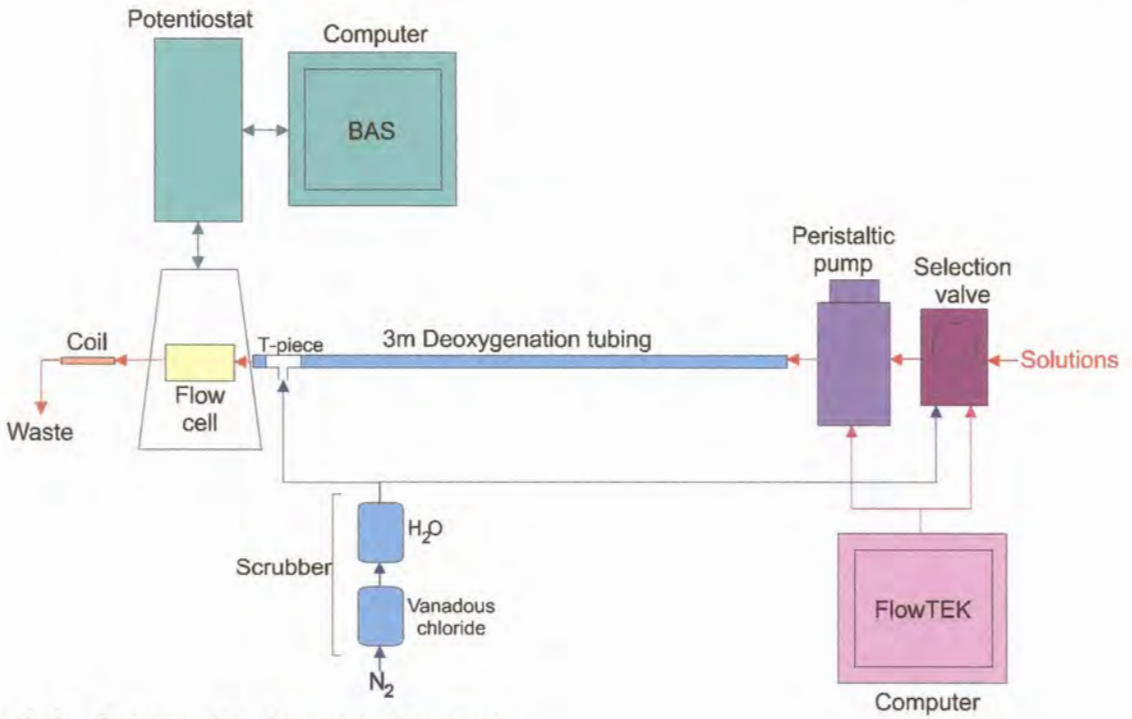

Figure 5.9: Schematic diagram of set-up

A Gilson Minipuls 3 peristaltic pump (Gilson, Villiers, France) and a VICI model EMHMA selection valve with the multiple-position actuator control module (Valco Instruments Co. Inc., USA) was used. The software used to control the pump and the valve was FlowTEK (Mintek, SA). The hardware needed for control was an interface card and a distribution board. The interface card used was an Eagle Electric PC-30B card (Eagle Electric, SA), which is a high accuracy analogue and digital input/output (I/O) board. It can be plugged into any of the fully bussed slots in an IBM or compatible computer. The distribution board (Mintek, SA) enabled the convenient connection of devices to the interface card. It also has optional features such as an amplifier and a filter [10]. FlowTEK could also be used to collect data, but it does not have the infrastructure for particular electrochemical experiments. The electrochemical experiments were done on a BAS 100B/W Electrochemical Workstation (Bioanalytical Sysytems, West Lafayette, USA) which was comprised of a potentiostat and a computer running the BAS software with a MS Windows interface. An EG&G Princeton Applied Research Model 303 SMDE (EG&G, New Jersey, USA) was used in the flow cell that was designed and was controlled by the BAS system.

Flow systems can be broadly classified as segmented and non-segmented systems. In a segmented flow system, solution plugs are separated by air or some inert gas [1,11]. This was initially done to prevent cross-contamination of samples, but it was later found that the extent of contamination was insignificant [11]. The system used here was a pseudo-segmented system as a nitrogen bubble was introduced after the matrix exchange solution, which directly proceeded the sample solution, in order to dislodge the mercury drop. Once the cell was rinsed with water, another nitrogen bubble was introduced so that the beginning of the sample plug could be seen. There was no bubble between the sample solution and the matrix exchange electrolyte or else the mercury drop would have been washed out of the cell after the plating step and before stripping could occur.

The presence of the nitrogen bubbles increased the compressibility of the contents in the tubing. When the pump was stopped, the solutions continued to flow for a short period thereafter. This was not adequate because a greater amount of control was needed over the positioning of the various solutions with respect to the flow cell. A coil of tubing with a small internal diameter was placed at the outlet of the flow cell to provide a back-pressure and improve control. On hindsight, the nitrogen slugs could also have been made smaller to reduce the extent of compressibility.

The use of a peristaltic pump in flow systems leads to periodic oscillations in the flow rate. This is particularly a problem for electrochemical detectors. For example, in voltammetric detectors the transfer of electroactive substance to the electrode surface must be done under reproducible, invariable transport conditions when measuring the current [12]. When a HMDE is used under pulsating flow conditions, it leads to irreproducible results. The pulsating flow causes the drop to vibrate and alters the geometry of the drop, as well as gives rise to different mass transport conditions [12].

Various methods have been used for pulse damping. An air chamber was introduced after the pump which acted as a pressure filter as shown in figure 5.10 [1,12]. A pump was placed at the outlet of the detector so that the solution is in effect drawn through [1]. Gas-driven systems have also been used to curb the problem of pulsation [1].

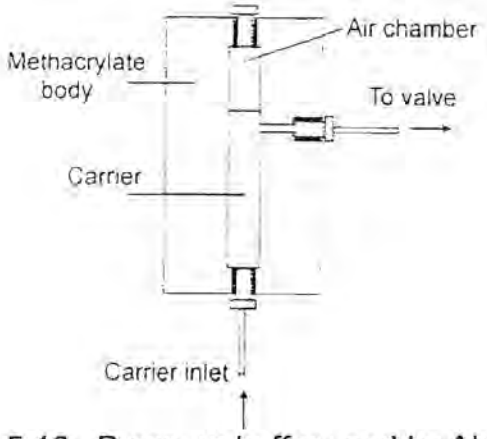

Figure 5.10: Pressure buffer used by Alpizar *et al.* [12]

In this study, a pulse damper consisting of a T-piece with a sealed piece of tubing on the vertical leg, as illustrated in figure 5.11, was introduced just after the pump. As the solution passed though the T-piece, the air in the sealed tube compressed and expanded thus reducing the pulsation. However, some problems were experienced with this pulse damper. The sealed tubing contained air which contaminated the nitrogen bubbles and solutions that passed though the damper, but this was a minor problem as the damper could be placed before the deoxygenation system. As the solution initially passed though the pulse damper, the air in the sealed tubing was compressed and some solution was pushed into this tube. This solution also vibrated as the solution flowed through the T-piece and a certain amount of mixing occurred. The most serious problem transpired when the solution was halted to do the stripping phase in a stationary solution in order to reduce the noise. The solution and some air would slowly creep back into the main tubing, causing contamination and air bubbles that would dislodge the mercury drop at inappropriate times.

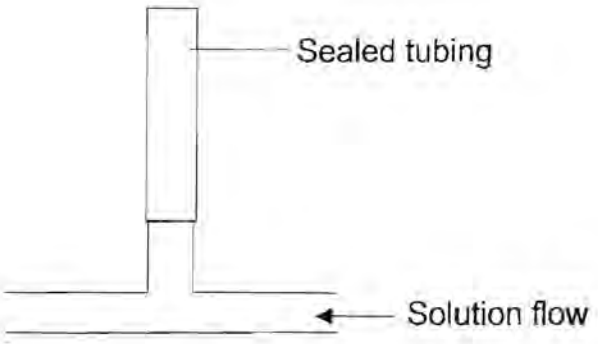

Figure 5.11: Pulse damper

It was found that, together with the solution having to pass through the 3m long deoxygenation tubing and with the coil placed at the outlet of the flow cell to provide a back pressure, the pulsation was reduced such that there was very little or no pulsation by the time the solution was pumped into the flow cell. The pulse damper could thus be omitted from the set-up.

Alternative flow system set-ups were considered with respect to the positioning of the components and the pro's and cons of these. Three examples are shown below.

1) The sample would be the only solution to flow through the deoxygenation tubing in the first alternative set-up, as shown in figure 5.12. The rinse solution and stripping electrolyte could be continuously purged by nitrogen in flasks as these solutions remained the same throughout the analyses. This would result in less dispersion as the solutions would have a shorter distance to travel while they were in contact with each other and there would be greater control over the positioning of the various solutions with respect to the flow cell. However, the solutions would be contaminated by oxygen when passing through the selection valve and the pump. A pulse damper would also be needed as the pump would be adjacent to the flow cell.

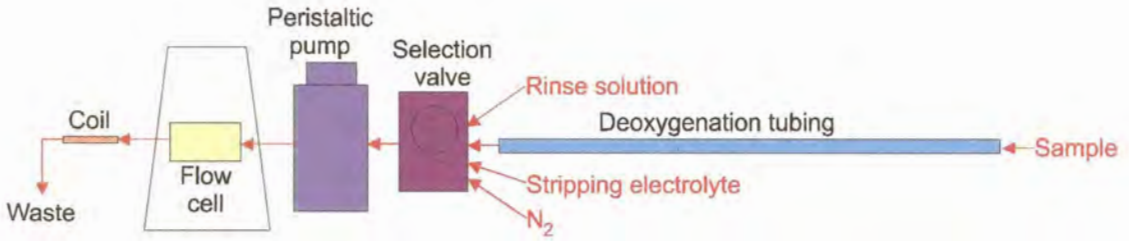

Figure 5.12: Alternative set-up 1

2) Placing the pump after the flow cell would result in the solutions being sucked through the system as depicted in figure 5.13. This would reduce pulsation and dispersion. The flow system would have to be thoroughly sealed to prevent air from being sucked into the system. This would not be the best option when using a HMDE as it could lead to fouling of the capillaries and affect the mercury flow.

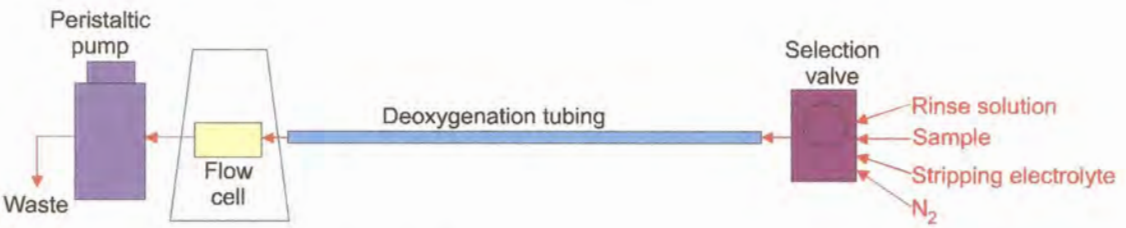

Figure 5.13: Alternative set-up 2

3) Introducing an injection valve was also considered, where the stripping electrolyte would be the carrier stream. A selection valve would also be needed to introduce the nitrogen to dislodge the mercury drop and a large sample loop would be required when long plating times were used. This would complicate the system and with the control that is afforded by using a program such as FlowTEK, the use of an injection valve does not provide considerable advantages.

5.3.2) Testing the Flow System

The flow system was tested to ensure that it would produce adequate and reproducible results.

5.3.2.1) Flow Rate

The flow rate was calibrated against the readings on the peristaltic pump by measuring the volume of solution that emerges from the system in a minute. The results are shown in table 5.2 and figure 5.14. It can be seen that the pump settings were directly proportional to the flow rates.

Table 5.2: Calibrating the Gilson peristaltic pump

Pump setting	**Flow rate / ml.min^{-1}**
10	1.5
20	2.9
30	4.4
40	5.8

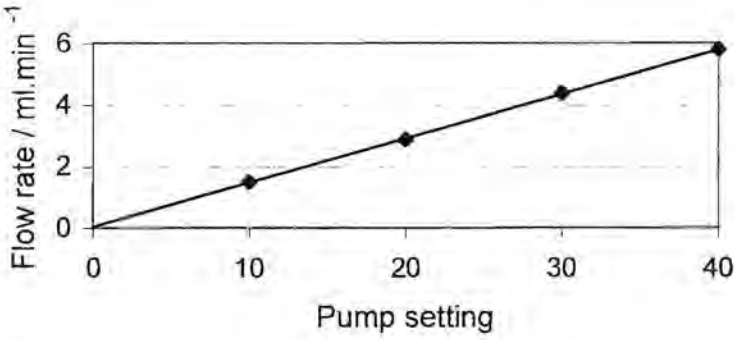

Figure 5.14: Graph flow rate of versus pump settings

5.3.2.2) Reproducibility

The reproducibility of the set-up was tested by measuring the peak height produced by a sample of 1 mg.l^{-1} copper (as $CuSO_4$) in 10% (v/v) nitric acid. A 5 s deposition time was used with a deposition potential of –300 mV. The mode applied was DPSV, with the scan rate set to 20 mV.s^{-1} and the final potential to 200 mV. The pulse amplitude was 50 mV, the pulse width was 50 ms, the sample width was 20 ms and the pulse period was 200 ms. During accumulation the flow rate was 1.5 ml.min^{-1} and stripping took place in a quiescent solution. The FlowTEK procedure (refer to section 5.3.3), shown in figure 5.15 below, allowed three sets of solutions to be stacked in the deoxygenation tubing at a time. The positions of the selection valve were as follows: position 1 was a water rinse, position 2 was the sample solution and position 3 was the nitrogen. The RSD obtained for 10 results was 3.5% which is

sufficient. The results also appeared to be random, in that the values obtained did not follow a trend.

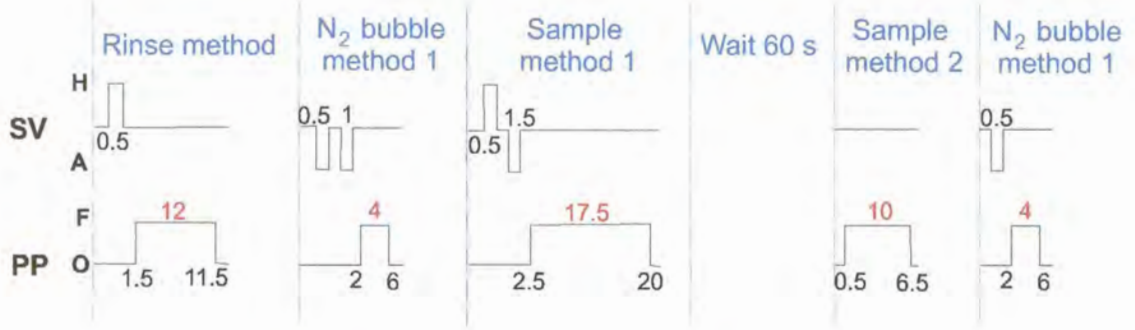

Figure 5.15: FlowTEK procedure for testing reproducibility

5.3.2.3) Flow Cell Characteristics

The characteristics of the flow cell were tested to see which cell type the designed cell best fits.

5.3.2.3a) *Effect of flow rate*

Firstly a copper solution was looked at where flow was maintained only during a 5 s plating step and then stripping was performed in a quiescent solution using the DPSV mode. The initial and final potentials were –200 mV and 120 mV respectively, and the deposition potential was –300 mV. The other conditions were as above. Deoxygenation took place through the membrane set-up.

The results given in table 5.3, were manipulated to ascertain which cell type the design fitted best. These results are also depicted in figure 5.16. The relationship between the peak current and the flow rate varies according to the cell type as was shown in table 5.1. It can be seen that for a planar electrode with perpendicular flow, the current in proportional to $(\text{velocity})^{1/2}$ and for a thin layer detector (TLD), the current is proportional to $(\text{volume flow rate})^{1/3}$.

Volume flow rate is given in units of $ml.min^{-1}$.

$$\frac{ml}{min} = \frac{cm^3}{s} \times \frac{60\ s}{1\ min}$$

$$\frac{cm^3}{s} \times \frac{1}{cm\ (diameter)} \times \frac{1}{cm\ (length)} = \frac{cm}{s}$$

Velocity is given in units of $cm.s^{-1}$. Since the diameter and the length of path are constant, it follows that the peak current is proportional to (volume flow rate)$^{1/2}$ for a planar electrode with perpendicular flow.

Table 5.3: The effect of flow rate on peak current

Pump speed setting	**Flow rate / ml.min^{-1}**	**(Flow rate)$^{1/2}$**	**(Flow rate)$^{1/3}$**	**Peak Current / μA**
5	0.8	0.894	0.928	0.4141
10	1.5	1.22	1.14	0.4193
20	2.9	1.70	1.43	0.4289

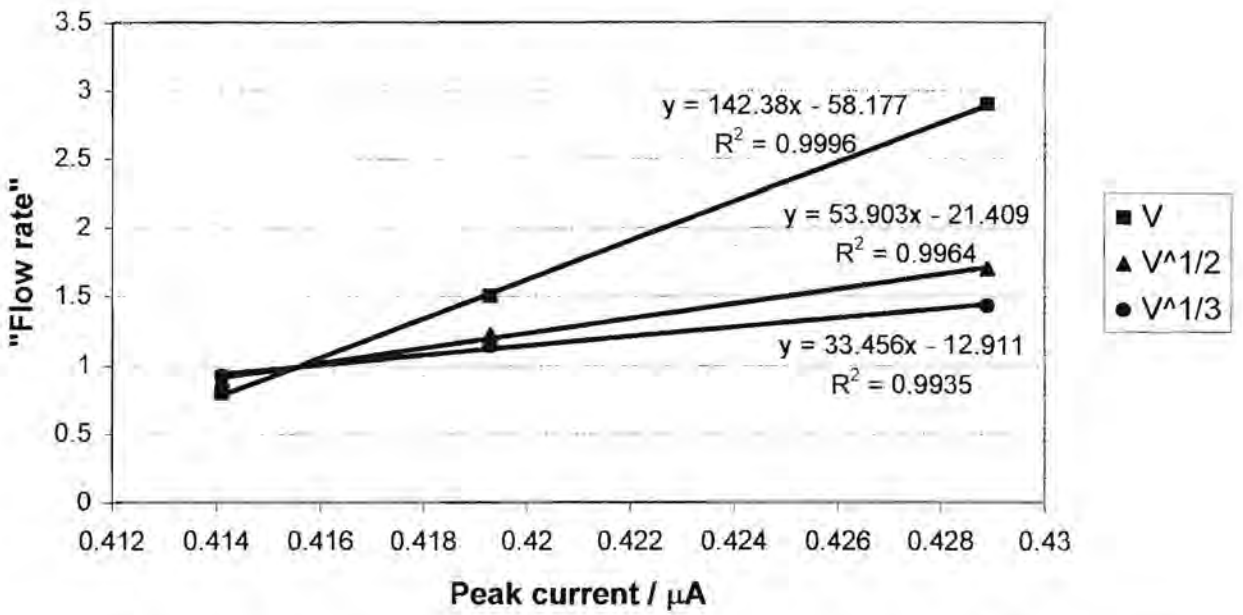

Figure 5.16: Graph of peak current versus flow rate, (flow rate)$^{1/2}$ and (flow rate)$^{1/3}$ for a 1 mg.l^{-1} copper solution deoxygenated in the tubing set-up

From figure 5.16 it could be deduced that a direct proportionality fitted the data best with a correlation coefficient of 0.9996. This did not correspond to either the TLD or a planar electrode with perpendicular flow.

It was, however, decided that passing the solution through the deoxygenation tubing would add another variable to the investigation, namely the extent of deoxygenation. In this case the slower the flow rate, the greater the residence time, hence the more the deoxygenation. Thus the solution was sparged in a flask before passing through a pulse damper (as described previously) and the flow cell. Data were collected in a manner similar to the previous experiments. The results obtained are shown in figure 5.17.

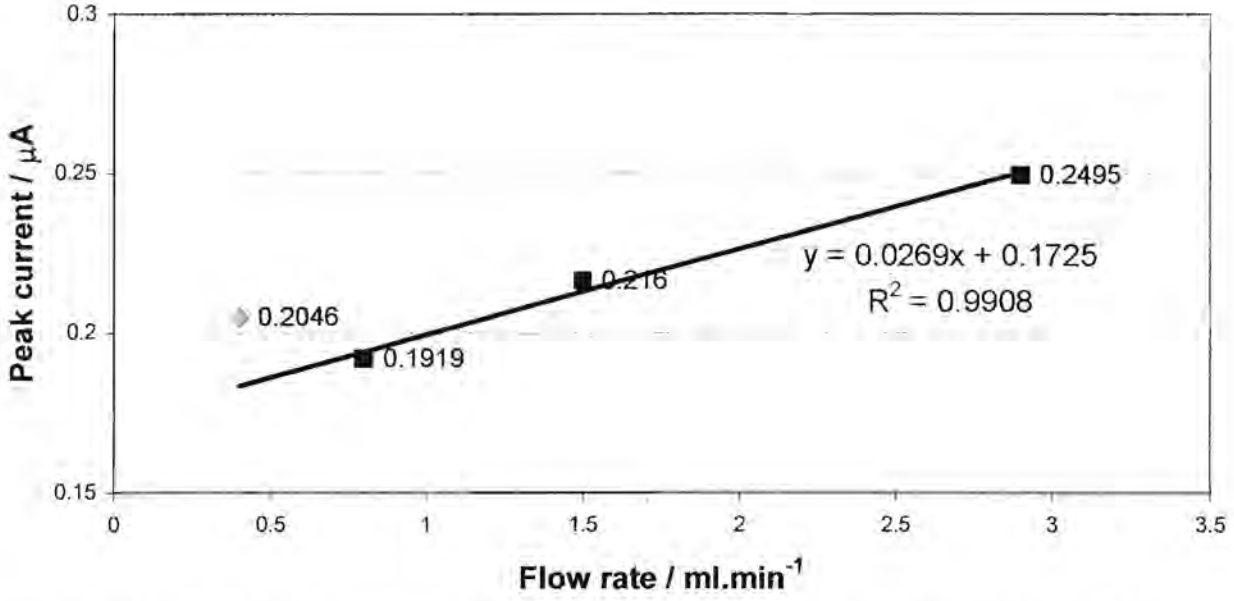

Figure 5.17: Graph peak current of versus flow rate for a 1 mg.l^{-1} copper solution deoxygenated in a flask

As the flow rate decreased, the peak current decreased in a linear manner, but then rapidly increased for the slowest flow rate of 0.4 ml.min^{-1}. The steady decrease in current was expected due to a decrease in mass transfer at slower flow rates, but the first datum point did not follow the trend. This could possibly show that there was laminar flow only at very low flow rates, and as the flow rates increased some turbulence set in. As the flow rate increased from there, the flow was still turbulent, but the increase in mass transport led to a slow increase in the peak current.

It was then decided not to use a stripping technique, but to simply use DPV in flowing solutions. A cadmium solution was used with no deoxygenation taking place, but still passing the solution through a pulse damper. The effect of oxygen present when

examining the cadmium reduction peak would be less than that for a copper peak as the first reduction peak for oxygen in close to that for copper. Data was collected from –300 to –800 mV at a rate of 10 $mV.s^{-1}$. The results obtained are presented in figure 5.18.

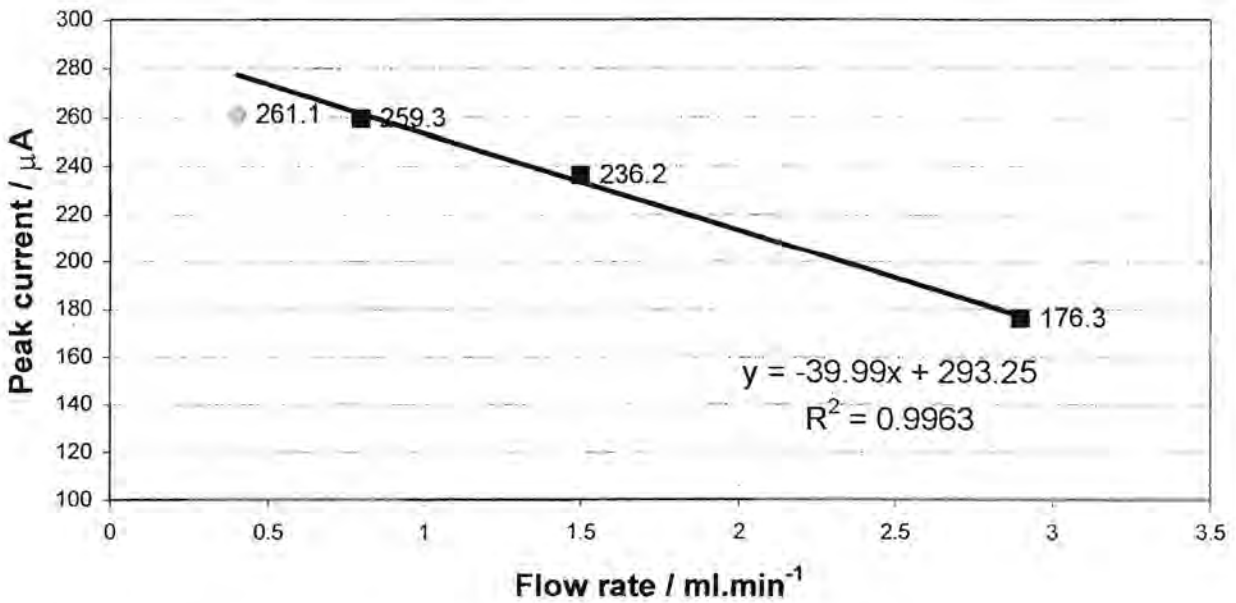

Figure 5.18 : Graph of peak current versus flow rate for a 1 $mg.l^{-1}$ cadmium solution with no deoxygenation

This produced totally unexpected results because the current was decreasing with increasing flow rate. It was later established that the faster the flow rate, the smaller the mercury drop was that formed in the flowing solution. At a flow rate of 5.8 $ml.min^{-1}$ a mercury drop did not form at all. The drop even became more unstable at low flow rates with time. This behaviour indicated that the capillary needed to be resiliconised. It appeared that the relatively large pressure led to the fast degradation of the capillary and would have to be examined periodically.

It was concluded that the hydrodynamics of the flow cell design did not fit into the category of either a thin layer detector or a planar electrode with perpendicular flow. Thus with the geometry of the flow cell being less well defined, the prediction of the absolute values of the current was not possible. A flow rate of 1.5 $ml.min^{-1}$ was used in the work from here on, unless stated otherwise. This would give a fair sensitivity due to the rate of mass transport and the mercury drop was stable at this flow rate.

5.3.2.3b) *Effect of scan rate*

The peak current was measured for varying scan rates in a cadmium solution. DPV was used and data was collected from –400 mV to –800 mV in a solution flowing at a rate of 1.5 ml.min^{-1}. The results are represented in figure 5.19.

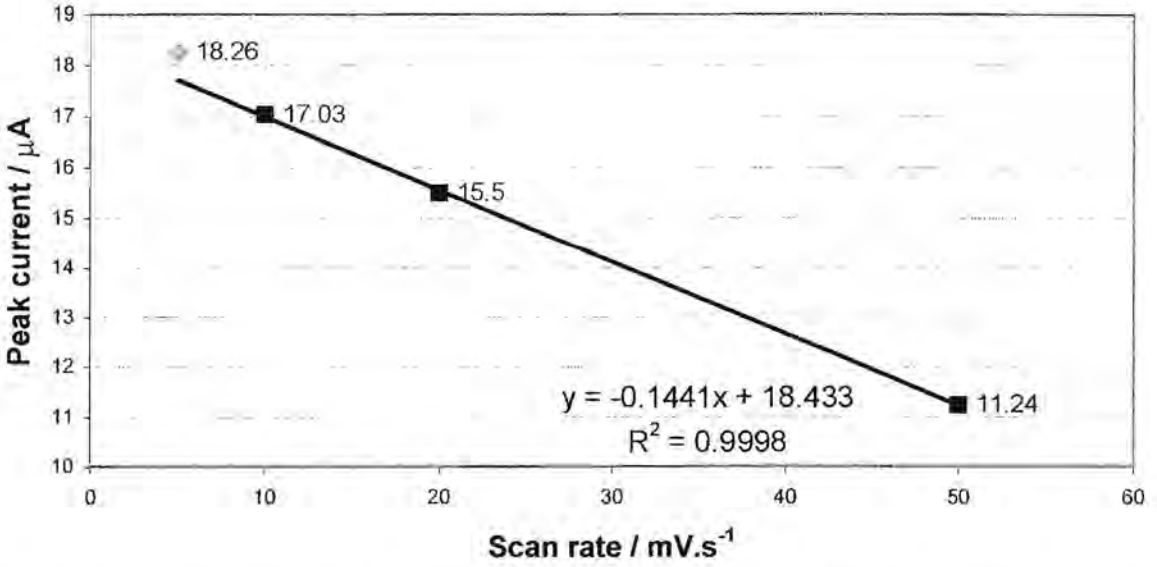

Figure 5.19: Graph of peak current versus scan rate for a 1 mg.l^{-1} cadmium solution

Data could not be collected at faster scan rates, as there were not enough data points for the software to calculate the peak height. Except for the scan rate of 5 mV.s^{-1}, the peak current decreased linearly with an increase in scan rate. A scan rate of 20 mV.s^{-1} was used in future work, unless stated otherwise, as this gave good sensitivity and also took a reasonable time for the run.

5.3.2.3c) *Effect of concentration*

The peak current was measured for various cadmium concentrations. Once again DPV was applied between –400 mV and –800 mV and data was collected in deoxygenated solutions flowing at a rate of 1.5 ml.min^{-1}. The voltammograms are shown in figure 5.20 and the results are depicted in figure 5.21.

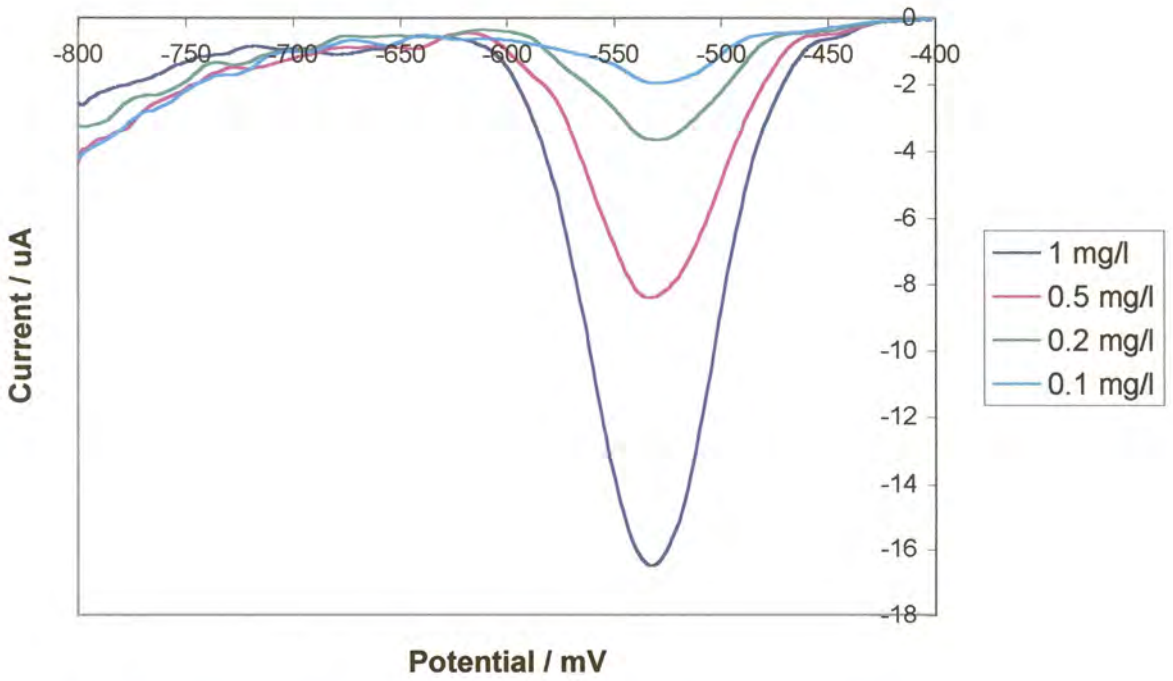

Figure 5.20: Voltammograms for varying cadmium concentrations

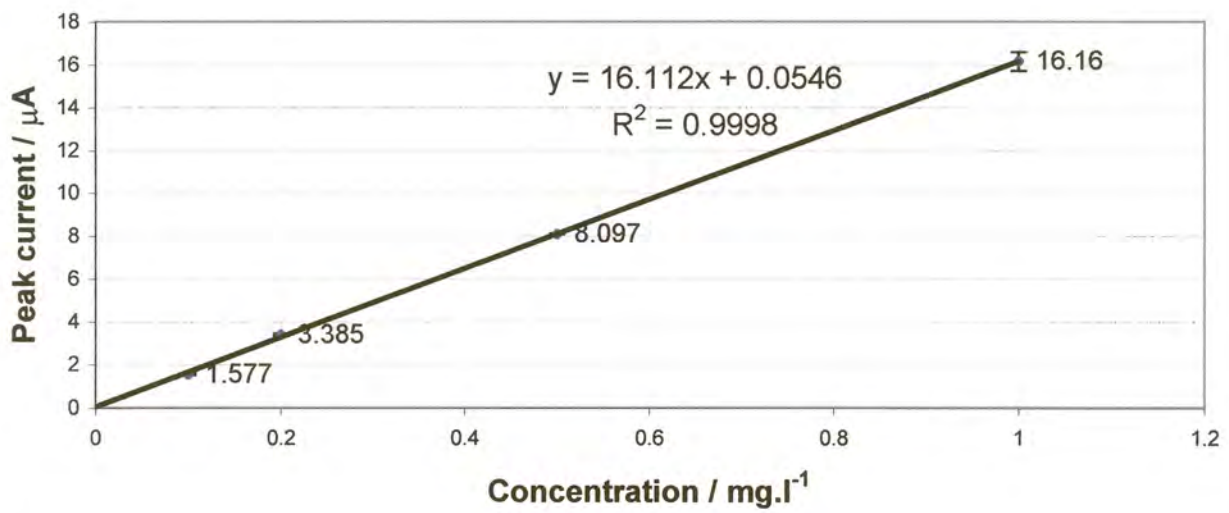

Figure 5.21: Graph of peak current versus concentration for a cadmium solution

This clearly shows a linear relationship between the concentration of the electroactive species and the peak current produced. This an important result when considering whether the design of the flow cell is feasible or not. Work was continued using the flow cell for determining cobalt in a zinc electrolyte.

5.3.3) FlowTEK Procedures

The FlowTEK software was used to control the peristaltic pump and the selection valve. This was done by first establishing the logic that controls the devices and then defining and configuring the devices (see the appendix). The actions that they could perform were then defined. In the case of the selection valve, the actions were "home", which took the valve to the first position, and "advance", which moved the valve one position forward. The valve could not move backwards, it had to first move to the home position and then move forward from there. The peristaltic pump's actions were "forward", "reverse" and "off", but the reverse option was not necessary for this work.

A method was built by specifying the time at which these actions must occur. A procedure could be built by arranging various methods in sequence and by replicating methods or procedures.

A typical FlowTEK procedure in this project for the determination of cobalt in a zinc electrolyte using matrix exchange is shown in figure 5.22. The solutions were arranged at the selection valve as follows: position1 (home) was water for rinsing, position 2 was nitrogen from the scrubber, position 3 was the sample solution and position 4 was the stripping electrolyte. The analytical procedure had several parts for one determination. Firstly the flow cell was rinsed with water and then a nitrogen bubble was passed through to indicate the start of the sample solution. The sample solution, that had been previously diluted with the supporting electrolyte, was pumped into the flow cell followed by the onset of accumulation of the analyte from a flowing solution. The stripping electrolyte was then introduced into the cell followed by a quiet time where the pump was halted and the solution was allowed to come to rest. Stripping of the analyte by a potential scan while measuring the current occurred in a quiescent solution before another nitrogen bubble was passed through to remove the used mercury drop from the cell.

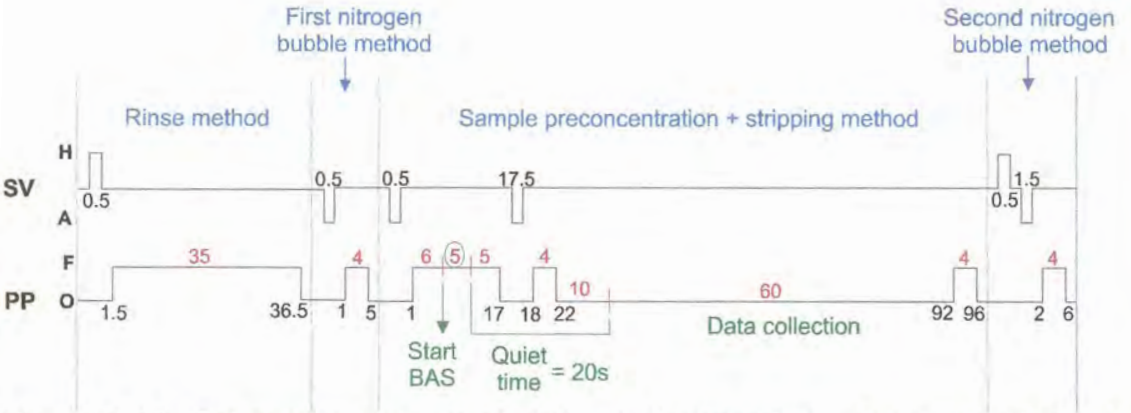

Figure 5.22: Schematic diagram of a FlowTEK procedure. SV = selection valve, H = home, A = advance, PP = peristaltic pump, O = off and F = forward.

The solutions were not pumped directly into the flow cell, but were first pumped through the 3 m long deoxygenation tubing. Due to the time delay, the samples for one determination were always stacked in the length of tubing. Thus as a particular solution was pumped into the tubing, the corresponding solution that was stacked in the tubing, was being pumped into the flow cell. As the accumulation time varied, the rinse time was adjusted to ensure that the tubing was always totally full.

The FlowTEK procedure in figure 5.22 needs some interpretation. The rinse method involved moving the selection valve to position 1 and then pumping water for 35 s. The first nitrogen bubble method shifted the valve to position 2 and pumped nitrogen for 4 s. The sample preconcentration and stripping step comprised moving the valve to position 3 to pump the sample solution through for 16 s. After pumping this solution for 6 s the cell was filled with the sample solution and the BAS system was started manually to apply the deposition potential for the accumulation step. The accumulation time was 5 s in this method and another 5 s of solution was allowed to flow through the cell to ensure that the cell only contained sample solution while accumulating analyte at the electrode. The valve was then shifted to position 4 and stripping solution was pumped for 4 s to ensure the cell contained stripping solution. An effective quiet time of 10 s then followed. The quiet time on the BAS system was given as 20 s, but this included the time to wash out the sample solution and fill the cell with stripping electrolyte. After data were collected in a quiescent solution, the stripping electrolyte was pumped for another 4 s. In effect a stripping electrolyte plug of 8 s was stacked in the tubing and was pumped halfway through the cell, thus

ensuring the whole cell was filled by stripping solution. Lastly, the selection valve was switched "back" to position 2 and another 4 s nitrogen bubble was pumped through.

5.4) FLOW SYSTEM FOR THE WJC

5.4.1) Set-up

The set-up used is represented in figure 5.23.

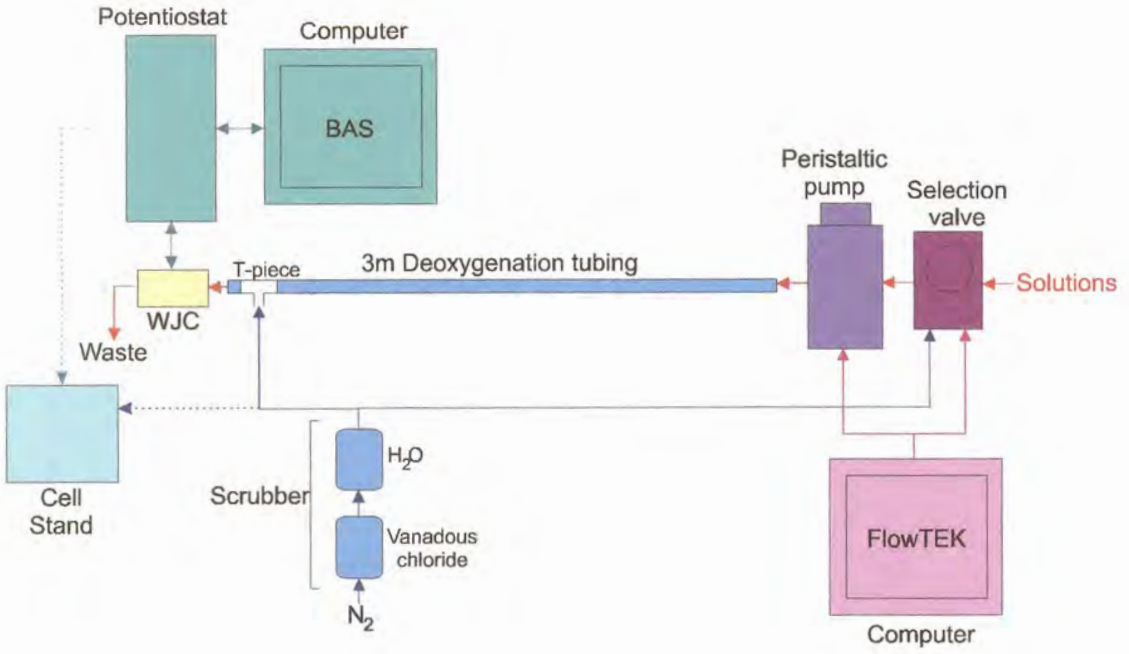

Figure 5.23: Schematic diagram of set-up

The same components as in the previous set-up were used, except the WJC was used and an Alitea C4 peristaltic pump (Alitea, Sweden) replaced the Gilson Minipuls 3 peristaltic pump during the course of this work as the latter pump stopped functioning. The BAS C2 Cell Stand (Bioanalytical Systems, West Lafayette, USA) was also used for the preparation of the gold film electrodes.

A non-segmented flow system was used throughout this work. It was necessary to first remove any air bubbles in the WJC when it was initially filled with solution. Once these bubbles were expelled, the solution would readily flow out of the two outlets at

a similar rate. The deoxygenation tubing once again acted as the pulse damper to prevent pulsating flow at the cell.

5.4.2) Testing the Flow System

5.4.2.1) Flow Rate

The Gilson peristalitc pump was recalibrated as different tubing was used and later the flow rate of the Alitea pump also required calibrating according to the pump settings. This was done as before. The results are displayed in table 5.4 and figure 5.24 for the Gilson pump and in table 5.5 for the Alitea pump.

Table 5.4: Calibrating the Gilson peristaltic pump

Pump setting	**Flow rate / ml.min^{-1}**
10	1.4
15	2.2
20	2.8
25	3.5
30	4.2
35	4.9
40	5.4

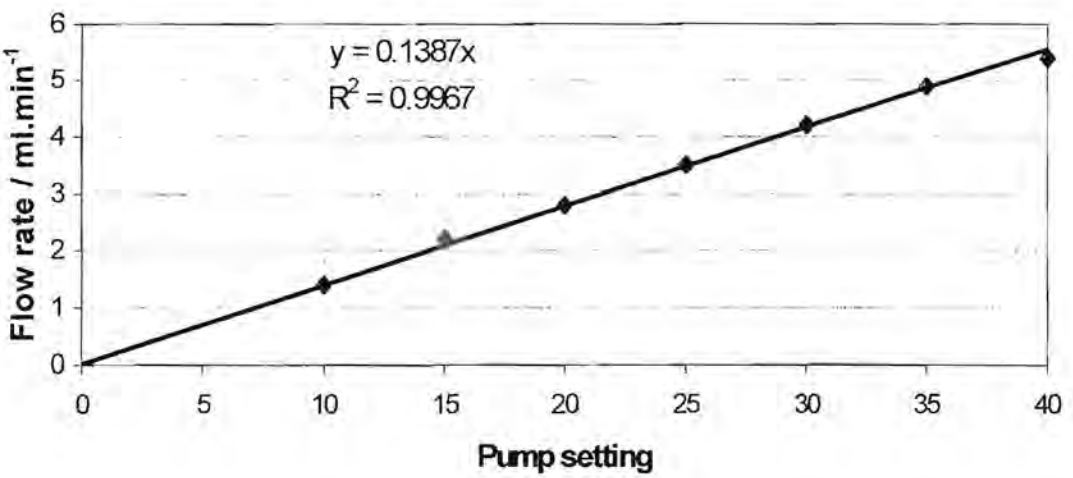

Figure 5.24: Graph of flow rate versus pump settings for the Gilson peristaltic pump

Table 5.5: Calibrating the Alitea peristaltic pump

Pump setting	**Flow rate / ml.min^{-1}**
30	1.3
90	3.9
95	4.0
98	4.2

5.4.2.2) Flow Cell Characteristics

The flow cell was investigated to determine which flow rates and inlet-electrode separations were required for the cell to exhibit wall-jet behaviour.

5.4.2.2a) *Effect of flow rate*

The WJC, with an inlet- electrode distance of 3 mm, was tested at flow rates of 2.8, 3.5 and 4.2 ml.min^{-1}. First a gold film electrode was prepared and a 10 mg.l^{-1} arsenic (III) solution in 20% (v/v) hydrochloric acid was analysed. DPSV was used from –300 mV to 400 mV at a scan rate of 50 mV.s^{-1} and a deposition time of 10 s. The other parameters were the default values of 50 mV pulse amplitude, 50 ms pulse width, 200 ms pulse period and 20 ms sample width. The results are presented in table 5.6. The peak current at the lowest pump speed was less than at the higher pump speeds. This could be due to the jet breaking up slightly before it reaches the electrode. The RSD was best for the highest pump speed. It was decided to work at a flow rate of 4.2 ml.min^{-1} which corresponded to the pump setting of 30 on the Gilson pump and 98 on the Alitea pump.

Table 5.6: Effect of flow rate on the peak current

Flow rate / ml.min^{-1}	**Peak current / μA**	**RSD / %**
2.8	11.4	7.3
3.5	12.5	1.7
4.2	12.2	0.4

5.4.2.2b) *Effect of inlet-electrode separation*

The limiting current is directly proportional to (flow rate)$^{3/4}$ for a WJE [13,14,15]. Therefore a plot of log(peak current) versus log(flow rate) should produce a straight

line of slope 0.75. Thus a 10 $mg.l^{-1}$ arsenic (III) solution in 20% (v/v) hydrochloric acid was analysed using LSV from –200 mV to 400 mV at a scan rate of 50 $mV.s^{-1}$. This was done for various inlet-electrode distances and the results are displayed in figure 5.25 and table 5.7. The greatest slope of 0.62 was for a 3.1 mm separation between the inlet and the electrode surface. Laevers *et al.* [1] suggested that for true wall-jet behaviour the relationship between the nozzle diameter (a) and the nozzle-electrode separation (H) should be:

$$12 \leq H/a \leq 15$$

With the nozzle diameter of 0.3 mm, it can be calculated that H/a = 3/0.3 =10. This does not fit in with the above relationship. A separation closer to 4 mm would give the required result. This would probably imply that the wall-jet was not fully developed when the solution struck the electrode surface. The results for the 2.9 mm separation produced a curve for which the best fit was not a linear relationship, but a polynomial. An inlet-electrode separation of 3 mm was used throughout this work. This distance was chosen as it produced a slope close to the maximum slope as shown in table 5.7.

Table 5.7: Table depicting the slopes and correlation coefficients for various inlet-electrode separations

Inlet-electrode separation / mm	**Slope**	**Correlation coefficient (R^2)**
2.9	0.47	0.9110
3.0	0.59	0.9986
3.1	0.62	0.9918
3.2	0.51	0.9990

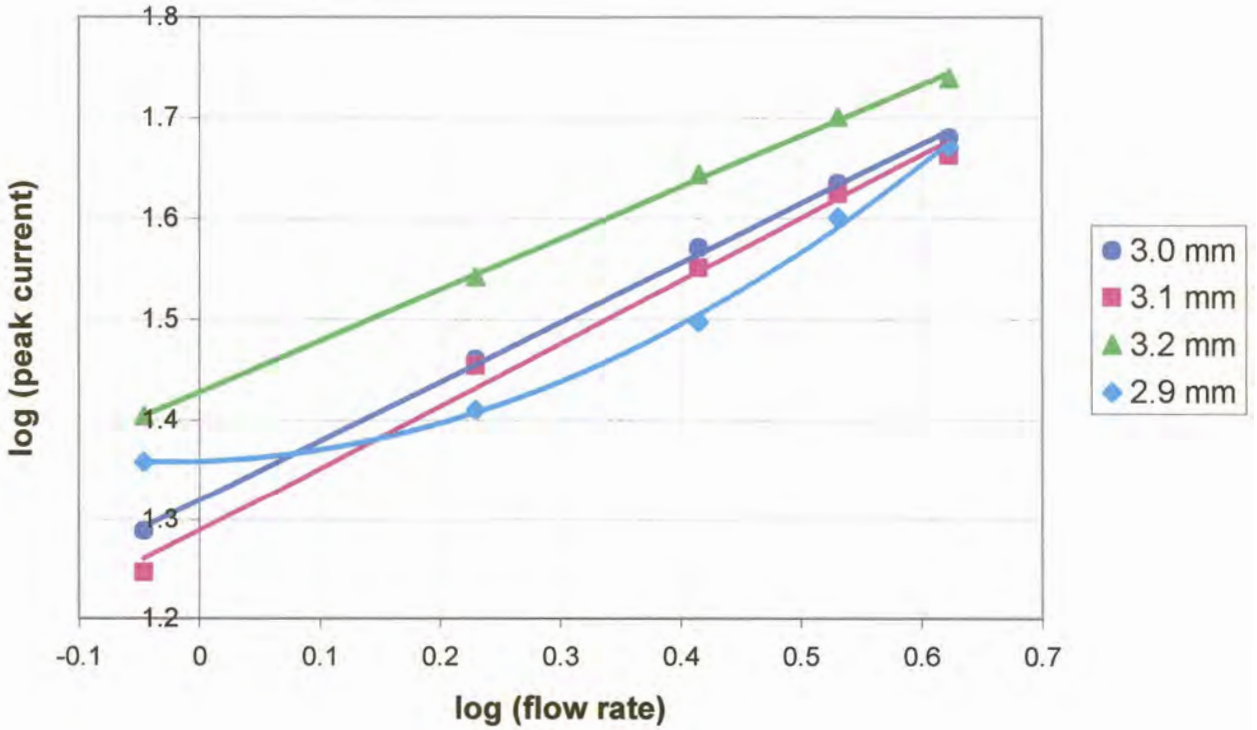

Figure 5.25: Graph of log(peak current) versus log(flow rate) at different inlet-electrode separations

5.4.3) FlowTEK Procedures

The FlowTEK software was once again used to control the peristaltic pump and selection valve as before. It took the solution 42 s to flow from the valve through the tubing to the flow cell when a flow rate of 4.2 $ml.min^{-1}$ was used. This interval affected the way in which the FlowTEK methods were created. Examples of procedures employed when matrix exchanged was used are described below.

Figure 5.26 depicts a FlowTEK method for a 20 s deposition time. Actually it is one method and then the start of the next, which is merely the same method that is repeated. This was done in order to clearly demonstrate what was happening at the various flow system components and how they influenced each other. The sample solution was at the first position and the stripping electrolyte was at the second position of the selection valve. The sample solution was pumped through the system for 42 s so that it was at the entrance of the flow cell when the valve was switched and the stripping solution was pumped through. As the stripping electrolyte was

pumped into the flow system, the sample solution flowed into the flow cell and the analyte could be collected at the electrode surface. A 12 s interval was given before accumulation began to ensure that unmixed sample solution was striking the electrode. Stripping solution flowed through the flow cell once sample solution was being pumped into the system again. Stripping occurred in a flowing solution because in a WJC, only the solution impinging on the electrode is seen by the electrode, not the bulk solution. This made it unnecessary to rinse the cell between analyses. The quiet time was introduced not in the true sense of the concept, as a quiet time is not necessary when using a WJE. Instead it allowed time for the excess sample solution to be pumped out of the deoxygenation tubing, the valve to be switched and to introduce the stripping electrolyte into the cell.

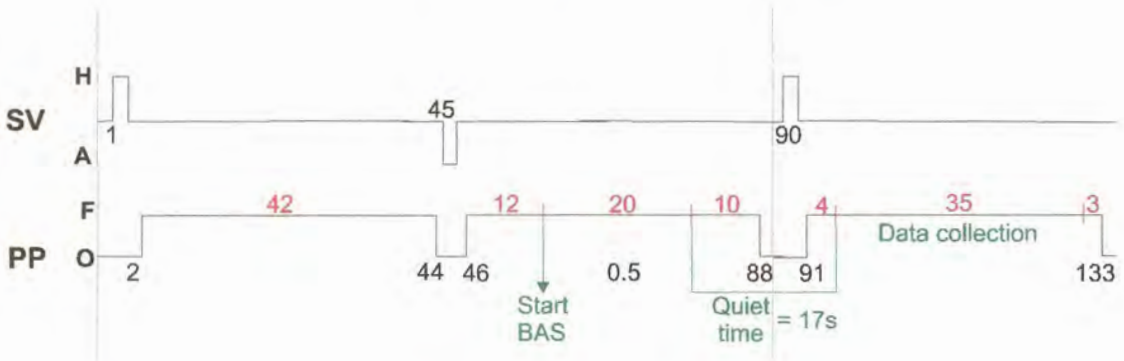

Figure 5.26: Schematic diagram of a FlowTEK method for a 20 s deposition time

Using longer deposition times such as 60 s changed the scenario as there was only space for 42 s worth of solution in the tubing at a time. Such a FlowTEK procedure is illustrated in figure 5.27. The first 42 s was spent loading the tubing with sample solution and thereafter it could be pumped through the flow cell for as long as required. When it came to stripping the analyte from the electrode in the stripping solution, the sample solution first had to be flushed from the tubing and the stripping electrolyte loaded. The quiet time encompassed this activity. Stripping could then take place in the flowing electrolyte. The data collection times for these two methods varied since it depended on the scan rate and the potential range used during this step.

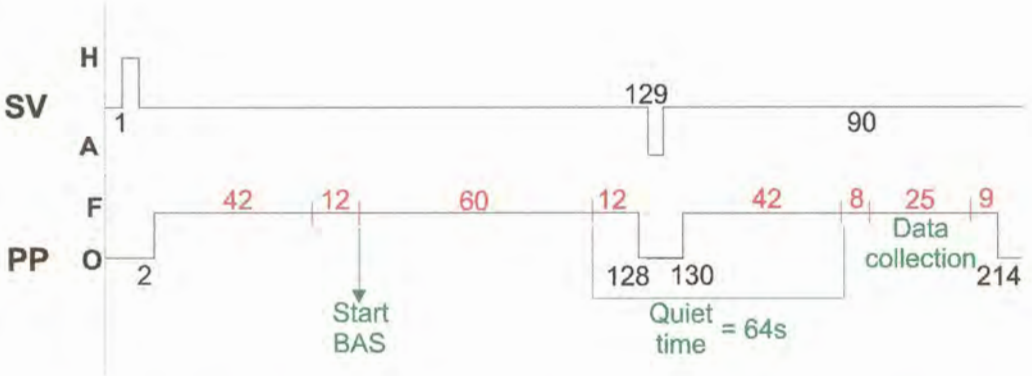

Figure 5.27: Schematic diagram of a FlowTEK method for a 60 s deposition time

If there were more than one sample to be analysed, it would probably be best to have the stripping electrolyte at position 1 and the sample solutions at the other positions. Thus after accumulation of the analyte, the valve would move to the home position and the stripping electrolyte will be pumped through the system.

5.5) REFERENCES

1) A.J. Bard, Electroanalytical Chemistry, Volume 16, Marcel Dekker Inc., 1989
2) H.B. Hanekamp and H.J. van Nieuwkerk, Anal. Chim. Acta, 121 (1980) 13
3) R.J. Rucki, Talanta, 27 (1980) 147
4) E.B. van Akker, M. Bos and W.E. van der Linden, Anal. Chim. Acta, 378 (1999) 111
5) E.A. Jones, Reference unknown
6) Z.-I. Zhi, Trends in Anal. Chem., 17 (1998) 411
7) BAS 100B/W Instrument Manual ,Version 2, 1995
8) F. Vydra, K. Stulik and E. Julakova, Electrochemical Stripping Analysis, Ellis Horwood Ltd, 1976
9) K.-N. Kuo, Communication received from BAS Inc: True iR compensation with the BAS-100 Electrochemical Analyzer
10) FlowTEK manual
11) W. Lund and L.-N. Opheim, Anal. Chim. Acta, 79 (1975) 35
12) J. Alpizar, A. Cladera, V. Cerda, E. Lastres, L. Garcia and M. Catasus, Anal. Chim. Acta, 340 (1997) 149

13) P. Laevers, A. Hubin, H. Terryn and J. Vereecken, J. Appl. Electrochem., 25 (1995) 1017

14) H. Gunasingham, K.P. Ang, C.C. Ngo, P.C. Thiak and B. Fleet, J. Electroanal. Chem., 186 (1985) 51

15) H. Gunasingham and B. Fleet, Anal. Chem., 55 (1983) 1409